



**HAL**  
open science

## Internal structure of basalt flows: insights from magnetic and crystallographic fabrics of the La Palisse volcanics, French Massif Central

T. Boiron, Jérôme Bascou, Pierre Camps, E.C. Ferré, C. Maurice, B. Guy, Marie-Christine Gerbe, P. Launeau

### ► To cite this version:

T. Boiron, Jérôme Bascou, Pierre Camps, E.C. Ferré, C. Maurice, et al.. Internal structure of basalt flows: insights from magnetic and crystallographic fabrics of the La Palisse volcanics, French Massif Central. *Geophysical Journal International*, 2013, 193 (2), pp.585-602. 10.1093/gji/ggs115. hal-00903561v1

**HAL Id: hal-00903561**

**<https://hal.science/hal-00903561v1>**

Submitted on 6 Mar 2015 (v1), last revised 19 Oct 2020 (v2)

**HAL** is a multi-disciplinary open access archive for the deposit and dissemination of scientific research documents, whether they are published or not. The documents may come from teaching and research institutions in France or abroad, or from public or private research centers.

L'archive ouverte pluridisciplinaire **HAL**, est destinée au dépôt et à la diffusion de documents scientifiques de niveau recherche, publiés ou non, émanant des établissements d'enseignement et de recherche français ou étrangers, des laboratoires publics ou privés.

# Internal structure of basalt flows: insights from magnetic and crystallographic fabrics of the *La Palisse* volcanics, French Massif Central

T. BOIRON<sup>1,2</sup>, J. BASCOU<sup>2</sup>, P. CAMPS<sup>3</sup>, E. C. FERRÉ<sup>4</sup>,  
C. MAURICE<sup>1</sup>, B. GUY<sup>1,2</sup>, M.-C. GERBE<sup>2</sup>, P. LAUNEAU<sup>5</sup>

<sup>1</sup>Ecole nationale supérieure des mines de Saint Etienne, 158 cours Fauriel, 42023 Saint Etienne, France

<sup>2</sup>Université de Lyon, UMR 6524 « Magmas et Volcans », CNRS and Université Jean Monnet, 23, rue du Dr. Michelon, 42023 Saint Etienne, France (E-mail : jerome.bascou@univ-st-etienne.fr)

<sup>3</sup>Géosciences Montpellier, UMR 5246, CNRS and Université de Montpellier, 34095 Montpellier, France

<sup>4</sup>Department of Geology, Southern Illinois University, Carbondale, IL 62901-4324, USA

<sup>5</sup>Laboratoire de Planétologie et Géodynamique, UMR 6112, CNRS and Université de Nantes, 2 rue de la Houssinière, 44322 Nantes, France

**Keywords:** basalt, columnar jointing, lava flow, magnetic anisotropy, inverse fabric, crystallographic preferred orientation, EBSD

## **Abstract:**

We present a new interpretation of anisotropy of magnetic susceptibility (AMS) fabrics in basaltic lava flows based on the detailed study of magnetic mineralogy and silicate crystallographic fabric of a Quaternary lava flow from the French Massif Central (La Palisse). We consider the model of AMS fabric imbrication between magnetic foliation and flow surface, as initially proposed for dikes. At the two sampling sites, the concordance between the flow direction deduced from the AMS foliation and that deduced from field observations indicates that the imbrication model could apply to the lava flows. However, the flow senses inferred from AMS are systematically opposed between the two sampling sites suggesting permutations between  $K_1$  and  $K_3$  AMS axes, a configuration referred to as inverse fabric. Electron backscatter diffraction (EBSD) measurements show strong lattice-preferred orientations (LPO) for plagioclase, especially the (010)-plagioclase plane, which tends to be parallel to the flow. Clinopyroxene LPO remains less marked than plagioclase LPO, whereas titanomagnetite does not display a significant LPO. Comparison between magnetic and crystallographic fabrics suggests that the AMS fabric of the lava flow results from the distribution of titanomagnetite grains, which is in turn controlled by the fabric of the silicate framework. Magnetic hysteresis parameters and anisotropy of remanent magnetization (ARM) measurements exclude a significant contribution from single-domain grains, often called upon to explain inverse magnetic fabrics. The origin of the observed inverse magnetic fabric may relate to the dip of the paleosurface, which is the only remarkable difference between the two sampling sites. AMS appears as a good tool to determine the direction of

40 basaltic lava flows and coupling with local crystallographic fabric data provides a valuable  
41 control of relationships between magnetic fabrics and flow and thus contributes to better  
42 constrain the AMS signature of lava flows.

43

## 44 **1. Introduction**

45 The internal structure of basaltic lava flows may provide key information on flow  
46 mechanisms and on lava rheology (e.g., Ventura et al., 1996; Smith, 2002). In general,  
47 macroscopic markers such as vesicles (e.g., Aubele et al., 1988) and measurement of lattice-  
48 preferred orientation (LPO) allow to investigate the internal structure of a flow (e.g., Long  
49 and Wood, 1986; Smith, 2002). However, the scarcity of markers in these rocks which are  
50 weakly anisotropic and the time-intensive nature of LPO measurements are significant  
51 hindrances to systematic studies of a flow from bottom to top.

52 The main goal of this study is to investigate if the anisotropy of magnetic susceptibility  
53 (AMS) technique can provide reliable information on internal structures and flow direction.  
54 The AMS technique has already been successfully used elsewhere to track both magmatic and  
55 deformation fabrics on a wide variety of rocks (e.g., Tarling and Hrouda, 1993; Borradaile  
56 and Henry, 1997; Bouchez et al., 2000; Ferré et al., 2003; Borradaile and Jackson, 2004),  
57 including volcanic rocks (e.g., Knight and Walker, 1988; Cañón-Tapia et al., 2004; Plenier et  
58 al., 2005; Loock et al., 2008; Petronis and Geissman, 2008). The significance of magnetic  
59 fabrics in volcanic rocks has been questioned because these rocks tend to show a weak  
60 magnetic anisotropy, near the detection limit of the AMS technique (Tarling and Hrouda,  
61 1993).

62 Despite the weak anisotropy of the volcanic rocks, AMS measurements show relationships  
63 between magnetic fabric and flow: maximum susceptibility axis  $K_1$  tend to be parallel to the  
64 flow direction and minimum susceptibility axis  $K_3$  tend to be perpendicular to the flow plane  
65 (Cañón-Tapia et al., 1996; Cañón-Tapia et al., 1997; Herrero-Bervera et al., 2001; Zhu et al.,  
66 2003; Cañón-Tapia et al., 2004; Raposo and Berquo, 2008). However complications have  
67 arisen regarding the significance of AMS fabrics and their relationship to magma flow  
68 directions (e.g., Rochette et al., 1999; Henry et al., 2003; Plenier et al., 2005).

69 In dike the imbrication model proposed by Knight and Walker (1988) considers that  $K_1$  and  
70  $K_3$  should be oblique and symmetrical with respect to the flow direction and flow plane. In  
71 this case, the obliquity further indicates the flow sense. This model often uses  $K_1$ -angle to

72 determine the flow direction (Staudigel et al., 1992; Herrero-Bervera et al., 2001). When the  
73 magnitudes of  $K_1$  and  $K_2$  axes are too close (oblate magnetic fabrics), a switch occurs between  
74 these two axes. The flow direction can be determined using the distribution of  $K_3$  axes (Callot  
75 et al., 2001; Geoffroy et al., 2002). Callot and Guichet (2003) also proposed an analytical  
76 model in dikes and concluded that the determination of the flow direction with the maximum  
77 susceptibility axis is a misuse, and recommend generalizing the magnetic foliation use.

78 Complications could also occur when single-domain (SD) magnetite grains are significant  
79 contributors to AMS (Potter and Stephenson, 1988). Indeed, in contrast to MD grains,  $K_1$  is  
80 parallel to the short axis and  $K_3$  is parallel to the long axis of SD grains. This generates an  
81 “inverse” magnetic fabric (Rochette et al., 1999; Ferré, 2002). Other difficulties to interpret  
82 the AMS signature could also appear due to magnetic interactions when the ferromagnetic  
83 (s.l.) grains are at close distance from each other (Grégoire et al., 1995; Fanjat et al., 2012),  
84 the effects of multiple mineral-preferred orientations (Hrouda, 1992), viscous strain variations  
85 in magma (Dragoni et al., 1997), post-flow alteration (Park et al., 1988) or thermal contraction  
86 (Gil-Imaz et al., 2006).

87 In basaltic lava flows, AMS is also used to infer the flow direction (e.g., Cañón-Tapia et al.,  
88 1996, 1997; Bascou et al., 2005; Looock et al., 2008). The imbrication model is used to  
89 determine the flow direction with either  $K_1$  or  $K_3$ . In lava flows, inverse fabrics are also  
90 observed (Rochette et al., 1999). Other parameters as chemical composition related to  
91 viscosity or paleosurface topography could influence the AMS fabrics (Cañón-Tapia et al.,  
92 1995; Merle 1998; Henry et al., 2003). In addition, the identification of relationships between  
93 AMS and the flow direction may depend on height in the flow. In their AMS study from  
94 basaltic lava flow, Bascou et al. (2005) observe a stronger correlation between AMS and  
95 flow-related plagioclase preferred orientation in the lower part of the lava flow than at other  
96 levels. Thus, the relationships between AMS and flow direction in a flow that could present  
97 variations from the base to the top in magnetic mineralogy, crystallographic and magnetic  
98 fabrics is still unclear.

99 In this study, AMS measurements were carried out on a Quaternary lava flow from the French  
100 Massif Central (La Palisse basaltic flow), which is exposed at different levels. A detailed  
101 study of the magnetic mineralogy has been carried out and relationships between AMS and  
102 the flow related silicate framework were investigated through 3-D crystallographic fabrics

103 characterization of main minerals (plagioclase, clinopyroxene and titanomagnetite) using  
104 electron backscatter diffraction (EBSD).

105

## 106 **2. Geological settings and petrology**

107 The La Palisse basaltic lava flow is located in the Bas-Vivarais volcanic province, in the East  
108 part of the French Massif Central (Fig.1a). The volcanic activity of the Bas-Vivarais province  
109 is characterized by alternated phreatomagmatic eruptions and strombolian activity and is  
110 spread over a large time interval, from  $166 \pm 15$  ka to  $45.4 \pm 3.2$  ka (Guérin and Gillot 2007).  
111 The La Palisse lava flow belongs to an eruptive episode occurring around  $78.8 \pm 5.3$  ka  
112 (Guérin and Gillot 2007). Its emission source is at the Suc de Bauzon scoria cone, from which  
113 the flow went NW into the Loire paleo-valley which was incised in the granitic substratum  
114 (Fig. 1b). The thickness of the flow is  $\approx 40$  meters at the sampling sites.

115 Two sampling sites were selected to address distinct structural levels of the flow. In sampling  
116 site 1, the colonnade and the entablature are clearly observed. The apparent thickness of the  
117 colonnade ranges from less than 1 m to about 3 m. Columns are vertical, oriented  
118 perpendicularly to the horizontal substratum surface and have a mean width of 0.4 m. In the  
119 entablature level, in which thickness ranges from 6 m to 12 m, columns are randomly oriented  
120 and only a few centimeters in width. In sampling site 2, three zones can be distinguished from  
121 base to top of (Fig. 2): the colonnade (from 1 to 3 m thick), an intermediate zone presenting  
122 planar layering and hereafter referred to as layered zone (from 1 to 2 m thick) and the pseudo-  
123 colonnade (From 2 to 4 m thick). The intermediate zone differs from the entablature level of  
124 site 1 by its planar structure. The strike of volcanic layers is NE-SW with a  $50^\circ$  dip to NW  
125 (Fig. 2). Because the La Palisse basalt flow is channeled by a paleo-valley, the underlying  
126 paleosurface, currently not outcropping, is assumed sub-horizontal at site 1 and parallel to the  
127 layered zone at site 2.

128 Regardless of the structural level, the lava flow samples contain phenocrysts and xenocrysts  
129 of olivine, phenocrysts of clinopyroxene, microphenocrysts (50 to 500  $\mu\text{m}$  in size) of  
130 plagioclase and a groundmass mainly composed of microlites of plagioclase, clinopyroxene  
131 and iron oxides within partially devitrified glass. The fluidal texture displayed by plagioclase  
132 microphenocrysts is observed in the different levels of the two sampling sites, whereas the  
133 pseudo-colonnade level exhibits a more vesicular texture.

134 The La Palisse lava is basanite (from TAS diagram, *Lebas et al.*, 1986), The mean  
 135 composition of phenocrysts are An50 for plagioclase, Fo78 for olivine and diopside for  
 136 clinopyroxene (*Boiron*, 2011). The oxide grains are mainly Ti-rich titanomagnetite ( $\text{Fe}_{3-x}\text{Ti}_x\text{O}_4$   
 137 with x mean value of 0.6; *Boiron*, 2011).

138

### 139 3. Methods

#### 140 3.1. Magnetic methods

141 The anisotropy of magnetic susceptibility (AMS) was measured with a KLY-3 instrument at  
 142 the University of Montpellier (France). Thermomagnetic experiments were mainly conducted  
 143 under argon atmosphere, with a CS4 furnace coupled to a MFK1 Kappabridge instrument at  
 144 the University of Saint Étienne (France). AMS in low magnetic field ( $< 1\text{mT}$ ) is  
 145 mathematically described as a symmetric second rank tensor, which can be geometrically  
 146 expressed as an ellipsoid with three principal susceptibility axes ( $K_1$ ,  $K_2$  and  $K_3$  with  $K_1 \geq K_2 \geq$   
 147  $K_3$ ). For magnetite, AMS is controlled by the shape-preferred orientation (SPO) of individual  
 148 grains or aggregates (*Rochette et al.*, 1992). Many parameters are usually employed to  
 149 describe the AMS fabric of rocks. In this paper, we used the bulk magnetic susceptibility  
 150  $K_m = (K_1 + K_2 + K_3)/3$ , the corrected degree of anisotropy (*Jelinek* 1981)

151  $P' = \exp\sqrt{\{2[(\eta_1 - \eta_m)^2 + (\eta_2 - \eta_m)^2 + (\eta_3 - \eta_m)^2]\}}$  where  $\eta_1 = \ln K_1$ ,  $\eta_2 = \ln K_2$ ,  
 152  $\eta_3 = \ln K_3$  and  $\eta_m = \sqrt[3]{(\eta_1 \cdot \eta_2 \cdot \eta_3)}$ , and the shape parameter (*Jelinek* 1981) defined as  
 153  $T = (2\eta_2 - \eta_1 - \eta_3)/(\eta_1 - \eta_3)$ . The  $P'$  parameter is used to quantify the degree of magnetic  
 154 anisotropy and  $T$  characterizes the AMS ellipsoid shape.  $T$  ranges from -1 (prolate shape) to  
 155 +1 (oblate shape). Magnetic hysteresis and first order reversal curve (FORC) were measured  
 156 on a Vibrating Sample Magnetometer Princeton Measurements 3900-04 at the University of  
 157 South Illinois, Carbondale (USA). The anisotropy of anhysteretic remanent magnetization (A-  
 158 ARM) measurements were carried out by three steps using a 2G cryogenic SQUID  
 159 magnetometer with an alternating field (AF) demagnetizer at the University of Montpellier  
 160 (France). The sample was first AF demagnetized along three perpendicular axes with a  
 161 maximum magnetic field of 170 mT. In a second time, an ARM is acquired along a direction  
 162 perpendicular to the last demagnetized axis with a bias direct field of 30  $\mu\text{T}$  and AF of 120  
 163 mT. In the third step, the induced ARM was measured. These three steps are repeated for 6  
 164 positions following the sequence, +X, +Y, +Z, -X, -Y, and -Z.

### 165 ***3.2. Lattice-preferred orientation (LPO) and shape-preferred orientation (SPO)*** 166 ***methods***

167 The LPO of plagioclase, clinopyroxene and titanomagnetite was measured by indexation of  
168 electron-backscattered diffraction patterns (EBSD) with a Zeiss Supra 55 VP SEM at the  
169 École nationale supérieure des mines of Saint-Étienne (France). EBSD patterns are generated  
170 by interaction of a vertical incident electron beam with a carefully polished thin section tilted  
171 at 70°. The diffraction patterns are processed and indexed in terms of crystal orientation using  
172 the CHANNEL5 software from HKL, Oxford Instruments. Crystallographic orientations were  
173 measured grain-per-grain using an accelerating voltage of 20 kV, a working distance of 15  
174 mm, a current intensity of 26  $\mu$ A and a pressure of 15 Pa. The diffraction images indexation  
175 was based on crystallographic data of respectively: Wechsler et al. (1984) for titanomagnetite,  
176 Wenk et al. (1980) for plagioclase and Bertolo et al. (1994) for clinopyroxene.

177 Image analysis was performed from sets of 6 digital photos on thin sections in polarized light  
178 with different angles (from 0° to 150°) using a binocular microscope equipped with color  
179 CCD in order to obtain images displaying a relatively wide surface of analysis. The sets of  
180 digitized images were then processed and the SPO was calculated using the Intercept software  
181 developed by Launeau and Robin (1996). The 2-D SPO is represented by an ellipse  
182 characterized by the shape ratio (SR = ratio of the ellipse long/short axes) and the angle ( $\alpha$ )  
183 between the ellipse long axis and the reference sample direction (X). The 3-D SPO  
184 corresponds to the best ellipsoid calculated from the combination of ellipses taken on three  
185 perpendicular sections following the procedure of Launeau and Robin (2005) modified by  
186 Launeau et al. (2010); see also <http://www.sciences.univ-nantes.fr/lpgnantes/SPO>.

187

## 188 **4. Magnetic mineralogy**

189 The mode of titanomagnetite grains, determined by image analysis and reflected-light  
190 microscopy, is about 3% in volume for each level in the flow (Fig. 3). Grains are subhedral in  
191 shape and exhibit a mean size around 15  $\mu$ m. The grains, observed through optical  
192 microscopy and SEM, appear free of exsolutions.

193 Thermomagnetic curves were performed on basaltic powder coming from sampling at  
194 different levels of the flow (Fig. 4). Curves are generally reversible and show a Curie  
195 temperature ( $T_C$ ) ranging from 100°C to 140°C. These low  $T_C$  attest of the high titanium

196 content of titanomagnetite, with an average composition of  $\text{Fe}_{2.4}\text{Ti}_{0.6}\text{O}_4$  (Dunlop and Özdemir  
197 1997; Lattard et al., 2006). This composition is in agreement with microprobe data.  
198 Thermomagnetic analyses further suggest that the titanomagnetite grains are rather  
199 homogeneous in composition

200 The hysteresis parameters were measured on 26 samples of the different levels from sites 1  
201 and 2. Hysteresis curves clearly indicate the dominance of ferromagnetic (s.l.) minerals. The  
202 hysteresis curves are simple, no wasp-waisted shape being observed (Fig. 5a). The data in a  
203 plot of  $(M_{rs}/M_s)$  versus  $(H_{cr}/H_c)$  lies in the PSD domain in agreement to data from other  
204 natural basaltic lava of similar composition with Ti-rich titanomagnetite (Fig. 5b; Hartstra  
205 1982; O'Donovan et al., 1986). According to Dunlop (2002), the PSD grain size range is  
206 narrower for Ti-rich titanomagnetite than for magnetite and could extend from approximately  
207 2 to 25  $\mu\text{m}$ . The observed hysteresis properties are ambiguous and could result from either an  
208 intermediate and homogeneous grain size between SD and MD grains, or from a mixture of  
209 various SD and MD grain sizes. In order to precise the potential contribution of single-domain  
210 grains, First Order Reveal Curves (FORC) diagrams were carried out on samples from site 1  
211 and 2. FORCs are expressed by contour plots of a two-dimensional distribution function and  
212 they provide an accurate mean to reveal information on the different components in a mixed  
213 magnetic mineral assemblage (Pike et al., 1999; Roberts et al., 2000). FORC diagrams  
214 obtained from 4 samples from the colonnade (08tb12 and 08tb18, site 1) and from the layered  
215 zone (08tb59 and 08tb68, site 2) are provided on Fig. 6. The outer contours diverge from the  
216  $H_u = 0$  axis and intersect the  $H_c = 0$  axis whereas the inner contours are less divergent. The  
217 absence of any central peak in the four FORC diagrams confirms a very small contribution of  
218 SD particles (Roberts et al., 2000) and suggests a dominating PSD + MD mixing in the  
219 samples.

220

## 221 **5. Anisotropy of Magnetic Susceptibility (AMS)**

### 222 *5.1. AMS scalar parameters*

223 For site 1, the anisotropy degree  $P'$  is higher in the entablature level ( $P'$  mainly ranges from  
224 1.03 to 1.11) than in the colonnade level ( $P'$  mainly ranges from 1.01 to 1.08) whereas the  
225 mean susceptibility  $K_m$  is lower in the entablature ( $K_m$  mainly ranges from  $4.1 \cdot 10^{-2}$  SI to  $5.3 \cdot$   
226  $10^{-2}$  SI) than in the colonnade ( $K_m$  mainly ranges from  $4.9 \cdot 10^{-2}$  SI to  $5.8 \cdot 10^{-2}$  SI; Fig. 7a). In  
227 the entablature level, the distribution of the shape parameter ranges around a value of  $T = 0$



228 (triaxial shape). On the other hand, the shape parameter is more scattered in the colonnade  
 229 (Fig. 7b). For site 2, the range of  $P'$  values of the pseudo-colonnade is narrower (around 1.03)  
 230 than for colonnade and layered zone, from 1.02 to 1.06 and from 1.01 and 1.08, respectively.  
 231 The mean susceptibility  $K_m$  is similar for the colonnade and the layered zone ( $5.0 \cdot 10^{-2} \text{ SI} <$   
 232  $K_m < 6.1 \cdot 10^{-2} \text{ SI}$ ) whereas it is lower in the pseudo-colonnade ( $4.3 \cdot 10^{-2} \text{ SI} < K_m < 5.0 \cdot 10^{-2}$   
 233  $\text{SI}$ ; Fig. 7c). The shape parameter  $T$  for the layered zone and the colonnade is scattered in  
 234 oblate and prolate domains with a larger number of data for the oblate shape. Pseudo-  
 235 colonnade mainly spans the oblate domain ( $0.2 < T < 0.7$ ; Fig.7d).

236

## 237 **5.2. AMS fabrics**

238 AMS fabrics measured in the different flow levels of sites 1 and 2 are presented on  
 239 stereograms in the geographic referential (Fig. 8). In all stereograms, the AMS eigenvectors  
 240 ( $K_1 \geq K_2 \geq K_3$ ) are well grouped with narrow confidence ellipse and therefore the mean of  
 241 principal susceptibility axes is statistically significant. The  $K_3$  axes for site 1 are particularly  
 242 well grouped and the mean  $K_3$  displays close strike and dip. Maximum and intermediate axes  
 243 are also well grouped but seem to be inverted between the colonnade and the entablature. For  
 244 site 2, the minimum susceptibility axes remain the most grouped for all levels. The orientation  
 245 of the mean principal susceptibility axes ( $K_1, K_2, K_3$ ) is similar in the colonnade and the  
 246 layered zone but different for the pseudo-colonnade.

247 The determination of flow direction and flow sense from AMS fabrics is obtained by means  
 248 of the imbrication of the magnetic foliation with a sub-horizontal paleosurface for site 1. For  
 249 site 2, the paleosurface is assumed to be parallel to the layered zone (NE-SW striking and  
 250  $50^\circ$  NW dipping; Fig. 8). The flow direction is given by the pole of the paleosurface plane and  
 251 the pole of magnetic foliation (i.e., the minimum principal axis  $K_3$ ). The angle between  $K_3$  and  
 252 the paleosurface defines the imbrication angle that allows determining the flow sense  
 253 (Geoffroy et al., 2002). For site 1, flow direction and flow sense deduced from AMS are  
 254 consistent with field observations, both for the colonnade and the entablature. Similarly, for  
 255 site 2 a good correlation between flow direction deduced from AMS for the colonnade and the  
 256 layered zone and from field observations is obtained. For the pseudo-colonnade, the  $K_3$   
 257 direction at high angle ( $> 50^\circ$ ) perpendicularly to the layered plane, in comparison to the  
 258 lower levels suggests an opposite imbrication located on the top of the flow. However, the  
 259 magnetic foliation for pseudo-colonnade is strongly tilted and the imbrication angle is less

260 clear for this level. In addition, it must be noted that the flow sense deduced from AMS for  
261 the colonnade and the layered zone is opposed to field observations. The expected AMS  
262 diagram for site 2 with respect to the field geological evidences and the coherent AMS  
263 measurements for site 1, suggest an inversion between the maximum and the minimum axis  
264 for the colonnade and the layered zone of site 2.

265

## 266 6. Magnetic and crystallographic fabrics

### 267 6.1. Lattice preferred orientation

268 The LPO of plagioclase, clinopyroxene and titanomagnetite are presented on equal area and  
269 lower hemisphere projections in the specimen reference framework for the colonnade and the  
270 entablature of site 1 (Fig. 9a) and for the colonnade, the layered zone and the pseudo-  
271 colonnade of site 2 (Fig. 9b, c). Density contours are expressed in multiple uniform  
272 distribution (MUD) using the software PFch5 developed by David Mainprice  
273 ([ftp://www.gm.univmontp2.fr/mainprice//CareWare\\_Unicef\\_Programs/](ftp://www.gm.univmontp2.fr/mainprice//CareWare_Unicef_Programs/), University of  
274 Montpellier, France). The fabric strength is expressed by the texture index  $J$  (Bunge 1982),  
275 which ranges from 1 in the case of random orientation to  $\infty$  in the case of an ideal single  
276 crystal.

277 Plagioclase presents the highest fabric strength ( $4.5 < J < 5.8$ ). The plagioclase (010)-plane  
278 systematically shows the strongest maximum of density. For site 1, (010)-maximum of  
279 density values of plagioclase from the colonnade and the entablature are 4.40 and 5.37,  
280 respectively. Lower maximum of density values are observed for (100)-plagioclase (3.68 and  
281 4.38) and (001)-plagioclase (2.24 and 2.81). For site 2, maximum of density values of (010)-  
282 plagioclase for the colonnade, the layered zone and the pseudo-colonnade are 4.91, 5.23 and  
283 4.81, respectively, while lowest value are observed for the (100) and (001)-plagioclase. The  
284 highest (010)-plagioclase maximum of density values are reached for the entablature of site 1  
285 and for the layered zone of site 2. The highest values of the plagioclase fabric strength  $J$  are  
286 also reached in these zones (5.5 in the site 1 entablature and 5.8 in the site 2 layered zone).  
287 However, the site 2 colonnade and pseudo-colonnade present high fabric strengths as well ( $J$   
288  $> 5$ ).

289 Clinopyroxene LPO is not as strong as plagioclase LPO with a fabric strength  $J$  that ranges  
290 from 3.35 to 3.70. Maximum of density values are generally lower than 3 except for the

291 entablature and the layered zone for which the (001) plane is higher (3.73 and 3.63,  
292 respectively).

293 Close relationships are observed between crystallographic planes of plagioclase and  
294 clinopyroxene: (100)-plagioclase tends to be parallel to (001)-clinopyroxene and (010)-  
295 plagioclase tends to be parallel to (100)-clinopyroxene for the two sites and at all levels.

296 Finally, no clear preferred orientation can be deduced from the LPO of titanomagnetite, even  
297 considering maximum of density values higher than 2. However, it can be noticed that [100]-  
298 titanomagnetite has the highest maximum of density compared to [111] and [110]-  
299 titanomagnetite, especially for the colonnade at both site 1 and 2 (maximum of density values  
300 of 2.30 and 2.49 respectively).

301

## 302 ***6.2. Comparison between magnetic and crystallographic fabrics***

303 In order to precise the relationships between the plagioclase crystallographic preferred  
304 orientations and the AMS, we compared the orientation of  $K_1$ ,  $K_2$  and  $K_3$  axes with the  
305 plagioclase crystallographic fabrics on samples representative of the different flow levels. The  
306 principal susceptibility axes, as well as the best axes (eigenvectors) and the maximum of  
307 density of (100), (010) and (001)-plagioclase were projected on lower hemisphere  
308 stereograms in the specimen referential (Fig. 10). For site 1, in both colonnade and entablature  
309 levels, a clear correlation appears between the maximum susceptibility  $K_1$  and the “Best Axis”  
310 of (100)-plagioclase, between the minimum susceptibility  $K_3$  and the “Best Axis” of (010)-  
311 plagioclase and between the intermediate susceptibility  $K_2$  and the “Best Axis” of (001)-  
312 plagioclase. For site 2, relationships are less obvious: (100)-plagioclase is related to  $K_3$  in the  
313 pseudo-colonnade, but related to  $K_2$  in the layered zone and (001)-plagioclase presents a clear  
314 correlation with  $K_2$  in the pseudo-colonnade and also with  $K_3$  (DM Pl) in the colonnade. The  
315 (010)-plagioclase “Best Axis” shows high orientation correlations with  $K_1$  in the three flow  
316 levels.

317

## 318 **7. Discussion**

### 319 ***7.1. Relation between AMS and flow***

320 The results of the present study show that the use of AMS to determine the flow direction,  
321 which is largely employed in dikes (e.g., Knight and Walker, 1988, Geoffroy et al., 2002;  
322 Hastie et al., 2011), is also efficient in lava flows. We can notice that neither the maximum of  
323 magnetic susceptibility axis itself nor the imbrication of the magnetic lineation allow to find a  
324 flow direction that fit with the flow direction deduced from field evidences. In accord with  
325 previous AMS studies of lava flows (Saint-Thibéry; Bascou et al., 2005), the magnetic  
326 foliation imbrication appears as the best mean to obtain an accurate flow direction. .  
327 Concerning the flow sense, our results are contrasted. For site 1, the flow sense deduced from  
328 AMS coincides with the field observations, whereas for site 2, they are systematically  
329 opposed. The flow sense deduced from AMS for site 2 appears to coincide with a permutation  
330 between the minimum and the maximum axes compared to site 1. The origin of the inversion  
331 of AMS axes is discussed in a following part.

332

### 333 *7.2. Origin of AMS*

334 Magnetic anisotropy of volcanic rocks can result from different intrinsic properties of  
335 minerals such as: magnetocrystalline anisotropy, shape anisotropy and a non-intrinsic  
336 property as the distribution anisotropy that could result from clustering of small and equant  
337 ferromagnetic grains (Hargraves et al., 1991). Petrographical observations indicate that the  
338 titanomagnetite grains, which are the main carrier of the AMS in the La Palisse basalt flow,  
339 are subhedral. As a consequence, shape anisotropy of individual grains can be neglected. In  
340 addition, titanomagnetite LPO is randomly oriented that excludes a magnetocrystalline  
341 anisotropy, in particular a preferred orientation of [100]-titanomagnetite that corresponds to  
342 the best magnetization axis (Dunlop and Özdemir 1997). For lava flow, experimental studies  
343 of Hargraves et al. (1991) indicate that AMS can be produced from an anisotropy distribution  
344 of ferromagnetic particles constrained by a silicate “template”.

345 Image analysis based on 2-D and 3-D images was performed in order to precise the  
346 relationships between crystallographic and magnetic fabrics. The shape ellipse from image  
347 analysis is shown for site 1 (colonnade) where AMS signature is coherent with field flow  
348 direction and sense and for site 2 (pseudo-colonnade) where an inversion between  $K_1$  and  $K_3$   
349 is observed relative to their plagioclase relationship in site 1 (Fig. 11).

350 For site 1, magnetic fabric, SPO and LPO of plagioclase show close relationships. The  
351 “magnetic lineation” ( $K_1$ ) is parallel to plagioclase-(100) “Best Axis” and also parallel to the  
352 lath of plagioclase alignment. The “magnetic foliation” (plane perpendicular to  $K_3$ ) is parallel  
353 to plagioclase-(010) and corresponds to the flow plane (Fig.11a). These relationships between  
354 magnetic and the related flow crystallographic preferred orientation of plagioclase are totally  
355 coherent with the crystal habitus ‘in lath’ of plagioclase. The tight relationships between the  
356 crystallographic (LPO and SPO) and magnetic fabrics strongly suggest that plagioclase laths  
357 mainly control the spatial distribution of titanomagnetite grains, carrier of the AMS. In  
358 addition, EBSD analyses show that clinopyroxene and plagioclase LPO are coaxial and  
359 therefore, both flow related. Plagioclase and clinopyroxene could constitute a silicate  
360 framework that constrains the spatial distribution of titanomagnetite grains. These results are  
361 in accordance with the experimental studies of Hargraves et al. (1991) and observations in  
362 natural flow by Bascou et al. (2005).

363 For site 2, magnetic and crystallographic fabrics are also coaxial. However, contrary to site 1,  
364 relationships between AMS and crystallographic axes differ between the different levels,  
365 except for  $K_1$  that systematically coincide to the (010)-plagioclase “Best Axis” (Fig.10). In the  
366 pseudo-colonnade (site 2), the relationship between crystallographic and magnetic fabric  
367 shows a permutation of  $K_1$  with  $K_3$  compared to those observed for site 1. The (100)-  
368 plagioclase “Best Axis” tends to be parallel to  $K_3$  and to the long axis of the shape fabric  
369 (SPO) and the (010)-plagioclase “Best Axis” tends to be parallel to  $K_1$  and the short axis of  
370 the shape fabric (Fig. 11b).

371

### 372 ***7.3. Inverse AMS fabrics of La Palisse flow***

373 Distinctive AMS fabrics from those measured for site 1, which are considered normal because  
374 of their agreement with field observations and relationships with plagioclase (and  
375 clinopyroxene) crystallographic fabrics, are observed in the different levels of site 2. For the  
376 colonnade and the layered zone of site 2, a systematic permutation of  $K_1$  and  $K_3$  axes could  
377 allow to define a flow sense conform to the field evidences. Such inversion between  $K_1$  and  
378  $K_3$  is defined as an inverse magnetic fabric. Such fabric has already been described in other  
379 contexts and several explanations have been proposed for their occurrence. For example,  
380 Rochette et al. (1999), Potter and Stephenson (1988) and Borradaile and Puumala (1989) have  
381 proposed that inverse fabrics result from the presence of Single Domain titanomagnetite

382 grains within the rocks. Crystallization of secondary magnetic oxides in residual magma or as  
383 a result of hydrothermal alteration has also been evoked to be at the origin of ferromagnetic  
384 SD grain crystallization and therefore of inverse fabrics (Archanjo et al., 2002).

385 In the La Palisse basalt flow, the absence of Single Domain grains is highlighted by hysteresis  
386 parameters and FORC diagrams, both indicating a large and homogenous grain size of  
387 ferromagnetic grains in the two sites and in all levels of the flow. Thus, the inverse magnetic  
388 fabrics cannot be explained by the presence of small SD magnetic grains. The great  
389 homogeneity in size and shape of the titanomagnetite grains also excludes crystallization of  
390 secondary oxides during hydrothermal alteration processes. In addition, electron microprobe  
391 and thermomagnetic curves indicate that Ti-rich titanomagnetite grains, which are the main  
392 carrier of AMS, are relatively homogeneous in composition in the whole lava flow. The  
393 magnetic mineralogy study of the La Palisse basaltic lavas tends to exclude the presence of  
394 SD ferromagnetic grains as the cause of the inverse fabric. However, as underlined by  
395 Chadima et al. (2009), several studies have shown obvious inverse fabric in dikes whereas the  
396 magnetic grain size study from hysteresis measurements did not reveal SD grains evidences  
397 (e.g., Callot et al., 2001; DeFrates et al., 2006). Chadima et al. (2009) proposed to measure the  
398 anisotropy of remanent magnetization (ARM) when the presence of SD grains is supposed. In  
399 case of inverse AMS fabric, ARM shows a permutation of AMS maximum and minimum  
400 directions. In order to check the presence of these SD grains in the La Palisse samples, ARM  
401 measurements were performed (Fig. 12). ARM fabrics of the studied samples are  
402 characterized by  $K_3$  parallel to  $A_3$  (minimum axis of ARM) and therefore indicate no  
403 permutation between ARM and AMS fabrics. These results confirm that inverse AMS fabric  
404 is not a consequence of SD grain occurrence.

405 Petrological and chemical study of the La Palisse basaltic lava flow (Boiron, 2011) don't  
406 show significant difference in composition between samples of sites 1 and 2. Thermomagnetic  
407 data confirm that the samples are very fresh, unaffected by post-emplacement alteration  
408 processes. Magnetic susceptibility is high but relatively similar for both sites, in particular for  
409 the colonnade ( $4.9 \cdot 10^{-2} \text{ SI} < K_m < 6.1 \cdot 10^{-2} \text{ SI}$ ). This point is important because a higher  
410 value of susceptibility to one of the sites could be associated with an increase of magnetic  
411 interactions due to a higher clustering of ferromagnetic grains, which could generate abnormal  
412 magnetic fabric (Fanjat et al., 2012). Various numerical and analogical modeling (Merle,  
413 1998; Cañón-Tapia and Pinkerton 2000; Cañón-Tapia, E. and Chávez-Álvarez, M., 2004)  
414 show that the shear intensity could impact on magnetic fabrics. When the shear is important,

415 the foliation development promotes an orientation of the minimum axis  $K_3$  perpendicular to  
416 the shear plane. On the contrary, in the case of weaker shear intensity, the magnetic fabric is  
417 preferentially lineated and the maximum axis  $K_1$  tends to be perpendicular to the shear plane.  
418 Elongation ration of the particles could also affect the orientations. It is particularly difficult  
419 to quantify in natural lava. However, images analysis from digital photos on thin sections  
420 does not show significant differences in grain size of minerals coming from similar areas  
421 (e.g., the top of the colonnade). In addition, neither the crystallographic fabric strength ( $J_{\text{index}}$ )  
422 of plagioclase, nor the magnetic anisotropy values ( $P'$ ) do not show strong variations between  
423 the both sites that suggests relatively comparable amount of shearing strain during the latest  
424 stages of the lava flow evolution.

425 A synthesis of data characterizing the studied sites of the La Palisse lava flow is presented in  
426 Figure 13. It clearly appears that the main difference between the both sites concerns the  
427 paleosurface slope, very gently for site 1 and high ( $50^\circ$ ) slope for site 2. Canon-Tapia et al.  
428 (1995, 1996, 1997) indicate that the morphology of a lava flow is strongly controlled by the  
429 rheology and the slope of the pre-existing terrain. The maximum of susceptibility axes are  
430 more scattered and sometimes even perpendicular to the flow direction when the slope of  
431 paleosurface is very weak whereas less scattered maximum axes are observed with a stronger  
432 slope. Numerical modeling of Merle (1998) shows that flowing over an inclined base  
433 produces complex stretch and flattening plane trajectories in the vertical plane and thus,  
434 generate significant gap between the stretching direction and the flow direction (and the  
435 associated fabric development).

436 Finally, the viscosity of the lava during emplacement can also have a great influence on the  
437 degree of anisotropy as shown by Hrouda et al. (2005). Such geological causes could explain  
438 the colonnade and the layered zone inverse fabrics of site 2.

439

## 440 **8. Conclusions**

441 In this AMS study, we show that the determination of the flow direction and the sense can be  
442 achieved through the use of the magnetic foliation imbrication, in particular at the base of the  
443 flow. Contrary to others studies that base the AMS analysis on the  $K_1$  directions (with or  
444 without imbrication), the measurements on the La Palisse lava flow highlight the poor

445 reliability of magnetic lineation. This can easily induce inversion between  $K_1$  and  $K_2$  during  
446 the flow.

447 EBSD data show clear correlations between plagioclase and clinopyroxene LPO: (100)-  
448 plagioclase tends to be parallel to (001)-clinopyroxene and (010)-plagioclase tends to be  
449 parallel to (100)-clinopyroxene. In addition, LPO orientations, and also shape preferred  
450 orientations of plagioclase show tight relationship with principal AMS directions. For site 1,  
451 (010)-plagioclase is parallel to the magnetic foliation ( $K_1$ ,  $K_2$ ) and coincides to the flow plane,  
452 and the pole of (100)-plagioclase is parallel to  $K_1$  and coincide the flow direction indicated by  
453 the preferred alignment of plagioclase laths. These close relationships between  
454 crystallographic and magnetic fabrics suggest a control of the silicate framework (plagioclase  
455 and clinopyroxene) on AMS carried by the titanomagnetite grains.

456 For both sampling sites (sites 1 and 2), the flow direction deduced from AMS is consistent  
457 with field evidences. However, only AMS in site 1 allows determining the geological flow  
458 sense. For site 2, the flow sense is systematically opposed to the geological flow sense.  
459 Relations between AMS and LPO are systematically different of those of site 1; for site 2, the  
460 pole of (010)-plagioclase is always parallel to  $K_1$  for the three levels, the pole of (100)-  
461 plagioclase is parallel to  $K_3$  for pseudo-colonnade, (001)-plagioclase tends to be parallel to the  
462 magnetic foliation ( $K_1$ ,  $K_2$ ) for colonnade whereas the layered zone do not indicate other clear  
463 relations.

464 Petrographic observation, thermomagnetic curves as well as hysteresis parameters indicate  
465 that magnetic minerals are mainly subhedral Ti-rich titanomagnetite grains belonging to Multi  
466 Domain and Pseudo-Single Domain. FORC diagrams exclude a grain size population  
467 dominated by single domain grain in the samples. Therefore, the permutation between  $K_1$  and  
468  $K_3$  axes cannot be related to the presence of SD grains that is confirming by ARM data.

469 Magnetic susceptibility parameters ( $P'$  and  $K_m$ ) are relatively similar for the two sites, except  
470 in the entablature of site 1 where the anisotropy degree ( $P'$ ) is higher than in the other levels.  
471 We also observe that the layered zone (site 2) is not the equivalent of the entablature (site 1),  
472 although both are located in the middle part of the flow. The crystallographic fabric strength  
473 ( $J_{\text{index}}$ ) of plagioclase (and clinopyroxene) is also relatively similar in the two sites.

474 The main difference between site 1 and site 2 concerns the paleosurface slope, very gently for  
475 site 1 and high ( $50^\circ$ ) slope for site 2 as indicated by the layered zone inclination and the tilt of



476 the columns. Inverse fabrics of site 2 may be then due to other factors than magnetic grain  
477 size such as viscosity or the paleosurface slope during the emplacement of the flow. However,  
478 additional analyses are needed to determine precisely which of these factors exerted the main  
479 control on the permutation of AMS axes.

480 If AMS appears as an efficient tool to reveal the structure of basalt flows and to deduce the  
481 flow direction, our study supports that inverse magnetic fabrics can occur even in the absence  
482 of Single Domain grains. Recently, Chadima et al. (2009) proposed to use preferably ARM  
483 rather than AMS fabric to determine flow direction and tectonic interpretations of magnetic  
484 fabric in dikes. However, this technique remains less usual than the measurement of AMS,  
485 which has become a common tool in rock magnetism. In lava flows, AMS measurements  
486 coupled with local analyses such as LPO obtained through EBSD technique or SPO deduced  
487 from image analysis could allow preventing misinterpretations based on AMS fabrics alone.

488

#### 489 **Acknowledgements**

490 The authors thank C. Cortial from the “Groupe géologique de la Haute-Loire” for his  
491 participation in the field prospection and B. Aneesa Lehman (Department of Geology,  
492 Southern Illinois University) for the hysteresis measurements. G. Hoareau and two  
493 anonymous reviewers are gratefully acknowledged for their valuable comments and remarks  
494 that have helped improving this paper.

495

#### 496 **References**

497 Archanjo, C., Araujo, M. and Launeau, P., 2002. Fabric of the Rio Ceará–Mirim mafic dike  
498 swarm (northeastern Brazil) determined by anisotropy of magnetic susceptibility and  
499 image analysis. *Journal of Geophysical Research*, 107(B3), 2046,  
500 doi:10.1029/2001JB000268.

501 Aubele, J.C., Crumpler, L. and Elston, W.E., 1988. Vesicle zonation and vertical structure of  
502 basalt flows. *Journal of Volcanology and Geothermal Research*, 35(4), 349-374.

503 Bascou, J., Camps, P. and Dautria, J., 2005. Magnetic versus crystallographic fabrics in a  
504 basaltic lava flow. *Journal of Volcanology and Geothermal Research*, 145(1-2), 119-  
505 135.

- 506 Bertolo, S., Nimis, P. and Dal Negro, A., 1994. Low-Ca augite from experimental alkali  
507 basalt at 18 kbar; structural variation near the miscibility gap. *American Mineralogist*,  
508 79(7-8), 668-674.
- 509 Boiron, T. (2011), Étude multi-échelle des variations structurales, géochimiques et des  
510 propriétés magnétiques des coulées basaltiques prismées : exemple de la coulée La  
511 Palisse (Ardèche) et de Saint-Arcons-d'Allier (Haute-Loire). PhD Thesis, École  
512 nationale supérieure des mines, Saint-Etienne, 279 pp.
- 513 Borradaile, G.J and Puumala, M., 1989. Synthetic magnetic fabrics in a plasticene medium.  
514 *Tectonophysics*, 164(1), 73-78.
- 515 Borradaile, G.J. and Henry, B., 1997. Tectonic applications of magnetic susceptibility and its  
516 anisotropy. *Earth-Science Reviews*, 42(1-2), 49-93.
- 517 Borradaile, G.J. and Jackson, M., 2004. Anisotropy of magnetic susceptibility  
518 (AMS), magnetic petrofabrics of deformed rocks. In: Martín-Hernandez, F.,  
519 Lünenburg, C.M., Aubourg, C., Jackson, M. (Eds.), Magnetic Fabrics. *Geological*  
520 *Society of London Special Publication No*, 238, 299-360.
- 521 Bouchez, J.-L., 2000. Anisotropie de susceptibilité magnétique et fabrique des granites.  
522 *Comptes Rendus de l'Académie des Sciences - Series IIA - Earth and Planetary*  
523 *Science*, 330(1), 1-14.
- 524 Bunge, H.J., 1982. Texture analysis in materials science, Butterworths London. 593 pp.
- 525 Callot, J.P., Geoffroy, L., Aubourg, C., Pozzi, J.P. and Mege, D., 2001. Magma flow  
526 directions of shallow dykes from the East Greenland volcanic margin inferred from  
527 magnetic fabric studies. *Tectonophysics*, 335(3-4), 313-329.
- 528 Callot, J.P. and Guichet, X., 2003. Rock texture and magnetic lineation in dykes: a simple  
529 analytical model. *Tectonophysics*, 366(3-4), 207-222.
- 530 Cañón-Tapia, E., Walker, G.P.L., and Herrero-Bervera, E., 1995. Magnetic fabric and flow  
531 direction in basaltic pahoehoe lava of Xitle Volcano, Mexico. *Journal of Volcanology*  
532 *and Geothermal Research*, 65, 249– 263.

- 533 Cãñón-Tapia, E., Walker, G.P.L and Herrero-Bervera, E., 1996. The internal structure of lava  
534 flows - Insights from AMS measurements.1. Near-vent a'a. *Journal of Volcanology*  
535 *and Geothermal Research*, 70(1-2), 21-36.
- 536 Cãñón-Tapia, E., Walker, G.P.L and Herrero-Bervera, E., 1997. The internal structure of lava  
537 flows - Insights from AMS measurements .2. Hawaiian pahoehoe, toothpaste lava and  
538 'a'(a)over-bar. *Journal of Volcanology and Geothermal Research*, 76(1-2), 19-46.
- 539 Cañón-Tapia, E. and Pinkerton, H., 2000. The anisotropy of magnetic susceptibility of lava  
540 flows: an experimental approach. *Journal of Volcanology and Geothermal Research*,  
541 98(1-4), 219-233.
- 542 Cañón-Tapia, E., 2004. Anisotropy of magnetic susceptibility of lava flows and dykes: A  
543 historical account. *Geological Society, London, Special Publications*, 238(1), 205-225.
- 544 Cañón-Tapia, E. and Chávez-Álvarez, M., 2004. Theoretical aspects of particle movement in  
545 flowing magma: implication for the anisotropy of magnetic susceptibility of dykes and  
546 lava flows. *Geological Society, London, Special Publications*, 238(1), 227-249.  
547
- 548 Chadima, M., Cajz, V. and Týcová, P., 2009. On the interpretation of normal and inverse  
549 magnetic fabric in dikes: Examples from the Eger Graben, NW Bohemian Massif.  
550 *Tectonophysics*, 466(1-2), 47-63.
- 551 Day, R., Fuller, M. and Schmidt, V.A., 1977. Hysteresis properties of titanomagnetites:  
552 Grain-size and compositional dependence. *Physics of the Earth and Planetary*  
553 *Interiors*, 13(4), 260-267.
- 554 DeFrates, J., Malone, D. and Craddock, J., 2006. Anisotropy of magnetic susceptibility  
555 (AMS) analysis of basalt dikes at Cathedral Cliffs, WY: implications for Heart  
556 Mountain faulting. *Journal of Structural Geology*, 28(1), 9-18.
- 557 Dragoni, M., Lanza, R. and Tallarico, A., 1997. Magnetic anisotropy produced by magma  
558 flow: Theoretical model and experimental data from Ferrar dolerite sills (Antarctica).  
559 *Geophysical Journal International*, 128(1), 230-240.
- 560 Dunlop, D.J. and Özdemir, Ö., 1997. *Rock Magnetism: Fundamentals and Frontiers*,  
561 Cambridge University Press, New York, 573 pp.

- 562 Dunlop, D.J., 2002. Theory and application of the Day plot (Mrs/Ms versus Hcr /Hc)1.  
563 Theoretical curves and tests using titanomagnetite data. *Journal of Geophysical*  
564 *Research*, 107(B3), 2057, doi:10.1029/2001JB000487.
- 565 Fanjat, G., Camps, P., Shcherbakov, V., Barou, F., Sougrati, M.T. and Perrin, M., 2012.  
566 Magnetic interactions at the origin of abnormal magnetic fabrics in lava flows: a case  
567 study from Kerguelen flood basalts, *Geophysical Journal International*, doi :  
568 10.1111/j.1365-246X.2012.05421.x.
- 569 Ferré, E.C. and Ameglio, L., 2000. Preserved magnetic fabrics vs. annealed microstructures in  
570 the syntectonic recrystallised George granite, South Africa. *Journal of structural*  
571 *geology*, 22(8), 1199-1219.
- 572 Ferré, E.C., 2002. Theoretical models of intermediate and inverse AMS fabrics. *Geophysical*  
573 *Research Letters*, 29(7), 1127, doi:10.1029/2001GL014367.
- 574 Ferré, E.C., Teyssier, C., Jackson, M., Thill, J.W., and Rainey E.S.G., 2003. Magnetic  
575 susceptibility anisotropy: a new petrofabric tool in migmatites. *Journal of Geophysical*  
576 *Research*. 108 (B2), 2086, doi:10.1029/2002JB00179.
- 577 Geoffroy, L. Callot, J.P., Aubourg, C. and Moreira, M., 2002. Magnetic and plagioclase linear  
578 fabric discrepancy in dykes: a new way to define the flow vector using magnetic  
579 foliation. *Terra Nova*, 14(3), 183-190.
- 580 Gil-Imaz, A., Pocovi, A., Lago, M., Gale, C., Arranz, E., Rillo, C. and Guerrero, E., 2006.  
581 Magma flow and thermal contraction fabric in tabular intrusions inferred from AMS  
582 analysis. A case study in a late-Variscan folded sill of the Albarracín Massif  
583 (southeastern Iberian Chain, Spain). *Journal of structural geology*, 28, 641– 653.
- 584 Grégoire, V., de Saint Blanquet, M., Nédeléc, A. and Bouchez, J.L., 1995. Shape anisotropy  
585 versus magnetic interactions of magnetite grains: Experiments and application to AMS  
586 in granitic rocks. *Geophysical Research Letters*, 22(20), 2765–2768.
- 587 Guérin, G. and Gillot, P., 2007. Nouveaux éléments de chronologie du volcanisme  
588 Pléistocène du bas Vivarais (Ardèche, France) par thermoluminescence. *Comptes*  
589 *Rendus Geosciences*, 339(1), 40-49.

- 590 Hargraves, R.B., Johnson, D. and Chan, C.Y., 1991. Distribution anisotropy: The cause of  
591 AMS in igneous rocks? *Geophysical Research Letters*, 18(12), 2193–2196.
- 592 Hartstra, R., 1982. Grain-size dependance of initial susceptibility and saturation  
593 magnetization-related parameters of 4 natural magnetites in the PSD-MD range.  
594 *Geophysical journal of the Royal astronomical society*, 71(2), 477-495.
- 595 Hastie, W.W., Watkeys, M.K. and Aubourg, C., 2011. Significance of magnetic and  
596 petrofabric in Karoo-feeder dykes, northern Lebombo. *Tectonophysics*, 513(1-4), 96-  
597 111.
- 598 Henry, B., Jordanova, D., Jordanova, N., Souque, C. and Robion, P., 2003. Anisotropy of  
599 magnetic susceptibility of heated rocks. *Tectonophysics*, 366(3-4), 241-258.
- 600 Henry, B., Plenier, G., and Camps, P., 2003. Post-emplacement tilting of lava flows inferred  
601 from magnetic fabric study : the example of oligocene lavas in the Jeanne d'Arc  
602 Peninsula (Kerguelen islands), *Journal of Volcanology and Geothermal Research*,  
603 127(1-2), 153-164.
- 604 Herrero-Bervera, E. Walker, GPL., Cañón-Tapia, E., Garcia, M.O., 2001. Magnetic fabric and  
605 inferred flow direction of dikes, conesheets and sill swarms, Isle of Skye, Scotland.  
606 *Journal of Volcanology and Geothermal Research*, 106(3-4), 195-210.
- 607 Hrouda, F., 1992. Separation of a component of tectonic deformation from a complex  
608 magnetic fabric. *Journal of Structural Geology*, 14(1), 65-71.
- 609 Hrouda, F. Chlupacova, M., Schulmann, K., Smid, J., and Zavada, P., 2005. On the effect of  
610 lava viscosity on the magnetic fabric intensity in alkaline volcanic rocks. *Studia*  
611 *Geophysica et geodaetica*, 49(2), 191-212.
- 612 Jackson, M., 1991. Anisotropy of magnetic remanence: A brief review of mineralogical  
613 sources, physical origins, and geological applications, and comparison with  
614 susceptibility anisotropy. *Pure and Applied Geophysics*, 136(1), 1-28.
- 615 Jelinek, V., 1978. Statistical processing of anisotropy of magnetic susceptibility measured on  
616 groups of specimens. *Studia geophysica et geodaetica*, 22(1), 50-62.
- 617 Jelinek, V., 1981. Characterization of the magnetic fabric of rock. *Tectonophysics*, 79(3-4),  
618 63-67.

- 619 Knight, M.D. and Walker, G.P.L., 1988. Magma Flow Directions in Dikes of the Koolau  
620 Complex, Oahu, Determined From Magnetic Fabric Studies. *Journal of Geophysical*  
621 *Research*, 93(B5), 4301–4319.
- 622 Lattard, D, Engelmann, R., Kontny, A., and Sauerzapf, U., 2006. Curie temperatures of  
623 synthetic titanomagnetites in the Fe-Ti-O system: Effects of composition, crystal  
624 chemistry, and thermomagnetic methods. *Journal of Geophysical Research-Solid*  
625 *Earth*, 111(B12)S28, doi:10.1029/2006JB004591.
- 626 Launeau, P. and Robin, P.-Y.F., 1996. Fabric analysis using the intercept method.  
627 *Tectonophysics*, 267(1-4), 91-119.
- 628 Launeau, P. and Robin, P.-Y.F., 2005. Determination of fabric and strain ellipsoids from  
629 measured sectional ellipses - implementation and applications. *Journal of Structural*  
630 *Geology*, 27, 2223-2233.
- 631 Launeau P., Archanjo C. J., Picard D., Arbaret L. and Robin P.-Y.F, 2010. Two- and three-  
632 dimensional shape fabric analysis by the intercept method in grey levels.  
633 *Tectonophysics*, 492, 230-239.
- 634 Lebas, M.J., Lemaitre, R.W., Streckeisen, A., and Zanettin, B., 1986. A Chemical  
635 Classification of Volcanic Rocks Based on the Total Alkali-Silica Diagram. *Journal of*  
636 *Petrology*, 27(3), 745 -750.
- 637 Long, P.E. and Wood, B.J., 1986. Structures, Textures, and Cooling Histories of Columbia  
638 River Basalt Flows. *Geological Society of America Bulletin*, 97(9), 1144-1155.
- 639 Loock, S., Diot, H., Van Wyk de Vries, B., Launeau, P., Merle, O., Vadeboin, F., and  
640 Petronis, M.S., 2008. Lava flow internal structure found from AMS and textural data:  
641 An example in methodology from the Chaîne des Puys, France. *Journal of*  
642 *Volcanology and Geothermal Research*, 177(4), 1092-1104.
- 643 Merle, O., 1998. Internal strain within lava flows from analogue modelling. *Journal of*  
644 *Volcanology and Geothermal Research*, 81(3-4), 189-206.
- 645 O'Donovan, J., Facey, D. and O'Reilly, W., 1986. The magnetization process in  
646 titanomagnetite (Fe<sub>2.4</sub>Ti<sub>0.604</sub>) in the 1-30 µm particle size range. *Geophysical*  
647 *journal of the Royal astronomical society*, 87(3), 897-916.

- 648 Park, J.K., Tanczyk, E.I. and Desbarats, A., 1988. Magnetic Fabric and Its Significance in the  
649 1400 Ma Mealy Diabase Dykes of Labrador, Canada. *Journal of Geophysical*  
650 *Research*, 93(B11), 13673–13687.
- 651 Petronis, M. and Geissman, J., 2009. Anisotropy of magnetic susceptibility data bearing on  
652 the transport of mid-tertiary regional ignimbrites, Candelaria Hills area, West-Central  
653 Nevada. *Bulletin of Volcanology*, 71, 121-151.
- 654 Pike, C., Roberts, A. and Verosub, K., 1999. Characterizing interactions in fine magnetic  
655 particle systems using first order reversal curves. *Journal of Applied Physics*, 85(9),  
656 6660-6667.
- 657 Plenier, G., Camps P., Henry B, Ildefonse B., 2005. Determination of flow directions by  
658 combining AMS and thin-section analyses: implications for Oligocene volcanism in  
659 the Kerguelen Archipelago (southern Indian Ocean). *Geophysical Journal*  
660 *International*, 160(1), 63-78.
- 661 Potter, D.K. and Stephenson, A., 1988. Single-domain particles in rocks and magnetic fabric  
662 analysis. *Geophysical Research Letters*, 15(10), 1097–1100.
- 663 Raposo, M. and Berquo, T., 2008. Tectonic fabric revealed by AARM of the proterozoic  
664 mafic dike swarm in the Salvador city (Bahia state): Sao Francisco Craton, NE Brazil.  
665 *Physics of the Earth and Planetary Interiors*, 167(3-4), 179-194.
- 666 Roberts, A.P., Pike, C.R. and Verosub, K.L., 2000. First-order reversal curve diagrams: A  
667 new tool for characterizing the magnetic properties of natural samples. *Journal of*  
668 *Geophysical Research*, 105(B12), doi:10.1029/2000JB900326.
- 669 Robin, P.-Y.F., 2002. Determination of fabric and strain ellipsoids from measured sectional  
670 ellipses – Theory. *Journal of Structural Geology*, 24, 531-544.
- 671 Rochette, P., Jackson, M. and Aubourg, C., 1992. Rock magnetism and the interpretation of  
672 anisotropy of magnetic susceptibility. *Reviews of Geophysics*, 30(3), 209–226.
- 673 Rochette, P., Aubourg, C. and Perrin, M., 1999. Is this magnetic fabric normal? A review and  
674 case studies in volcanic formations. *Tectonophysics*, 307(1-2), 219-234.
- 675 Smith J. V., 2002. Structural analysis of flow-related textures in lavas. *Earth-Science*  
676 *Reviews*, 57, 279-297.

- 677 Staudigel, H., Gee, J., Tauxe, L., Varag, R.J, 1992. Shallow intrusive directions of sheeted  
678 dikes in the Troodos ophiolite: Anisotropy of magnetic susceptibility and structural  
679 data. *Geology*, 20(9), 841-844.
- 680 Stephenson, A., Sadikun, S. and Potter, D., 1986. A theoretical and experimental comparison  
681 of the anisotropies of magnetic susceptibility and remanence in rocks and minerals.  
682 *Geophysical Journal of the Royal Astronomical Society*, 84(1), 185-200.
- 683 Tarling, D.H. and Hrouda, F., 1993. *The Magnetic Anisotropy of Rocks*, Chapman and Hall,  
684 London, 217 pp.
- 685 Ventura, G., De Rosa, R., Colleta, E. and Mazzuoli R., 1996. "Deformation patterns in a high-  
686 viscosity lava flow inferred from the crystal preferred orientation and imbrication  
687 structures: an example from Salina (Aeolian Islands, southern Tyrrhenian Sea, Italy).  
688 *Bulletin of Volcanology* 57, 555-562.
- 689 Wechsler, B.A., Lindsley, D.H. and Prewitt, C.T., 1984. Crystal structure and cation  
690 distribution in titanomagnetites (Fe (sub 3-x) Ti x O4). *American Mineralogist*, 69(7-  
691 8), 754-770.
- 692 Wenk, H.R., Lindsley, D. and Prewitt, C.T., 1980. The average structure of An 62-66  
693 labradorite. *American Mineralogist*, 65(1-2), 81-95.
- 694 Zhu, R., Shi, C. and Liu, Q., 2003. Anisotropy of magnetic susceptibility of Hannuaoba  
695 basalt, northern China: constrain on the vent position of the lava sequences.  
696 *Geophysical Research Letters* 30 (2), 1066, doi:10.1029/2002GL016215.
- 697



698 **Figure Captions:**

699 **Figure 1:** Location of the La Palisse basalt flow. (a) Location of the Bas-Vivarais volcanic region.  
 700 Black area refers to the volcanic provinces of the French Massif Central, (b) Geological map of the  
 701 studied area. Black arrows indicate the flow direction. The location of studied sites is also indicated.  
 702 GPS data: Site 1: N 44°47.38', E 4°05.33', Site 2: N 44°46.88', E 4°06.32'.

703 **Figure 2:** Photo of the La Palisse village outcrop (site 2) showing the colonnade, the layered zone and  
 704 the pseudo-colonnade levels within the lava flow.

705 **Figure 3:** Reflected light photomicrograph of representative thin section from the colonnade of the La  
 706 Palisse basalt flow (08tb14b sample; site 1). The white spots are mainly constituted of titanomagnetite  
 707 grains (Ti-Mt). Pl = plagioclase, Px = pyroxene, Ol = olivine.

708 **Figure 4:** Magnetic susceptibility ( $K/K_0$ ) versus temperature for representative samples from the  
 709 different levels of the La Palisse basalt for site 1 and 2. The thermomagnetic curves are commonly  
 710 reversible and the rapid change in susceptibility indicates a Curie temperature ( $T_c$ ) of about 110°C  
 711 associated to the Ti-rich titanomagnetite grains. Thermomagnetic curves determination under argon  
 712 atmosphere at heating rate of 11°C min<sup>-1</sup>.

713 **Figure 5:** a) Representative hysteresis curves (magnetic moment,  $m$  versus applied field,  $H$ ) indicating  
 714 the presence of ferromagnetic (s.l.) grains. b) Mrs/Ms ratio versus Hcr/Hc ratio diagrams of samples  
 715 from the different levels of site 1 (LP site 1) and site 2 (LP site 2). Mrs: saturation remanence; Ms:  
 716 saturation magnetization; Hcr: remanent coercive force; Hc: ordinary coercive force. The limits of the  
 717 pseudo-single domain of titanomagnetite (TM60) are defined from Dunlop (2002). Titanomagnetite  
 718 experimental data are reported from Day et al. (1977). Titanomagnetite grains belong to the pseudo-  
 719 single domain (PSD) are consistent with data, also reported, from natural Ti-rich titanomagnetites  
 720 (O'Donovan et al., 1986; Hartstra et al., 1982). Numbers indicate the grain size in micrometers, C  
 721 (coarse grain) and F (fine grain) for experimental data.

722 **Figure 6:** FORCs diagrams from site 1 colonnade (samples 08tb12 and 08tb18) and from site 2  
 723 layered zone (samples 08tb59 and 08tb68). These diagrams are characteristic of Pseudo-Single  
 724 Domain + Multi Domain grains mixing.

725 **Figure 7:** Diagrams representing the anisotropy parameter  $P'$  versus the bulk magnetic susceptibility  
 726 ( $K_m$ ) for the different levels of site 1 (a) and site 2 (c). Diagrams of  $P'$  versus the shape parameter  $T$   
 727 are shown in (b) and (d) for site 1 and site 2, respectively.

728 **Figure 8:** Equal area projection in the lower hemisphere and geographical referential of the principal  
 729 magnetic susceptibilities axes ( $K_1$ ,  $K_2$ ,  $K_3$ ) measured in specimens from the different levels of the La  
 730 Palisse flow for sites 1 and 2. The flow direction inferred from field observations is shown by the  
 731 black arrow and the flow direction determined from AMS study is shown by the white arrow. The  
 732 confidence ellipses are computed from Jelinek's statistics (Jelinek, 1978).  $N$  = number of  
 733 measurements. For site 2, the layered flow plane is also presented in full line for layered zone and in  
 734 dashed line for colonnade and pseudo-colonnade.

735 **Figure 9:** Lattice Preferred Orientation (LPO) of plagioclase, clinopyroxene and titanomagnetite of  
 736 samples from the different levels of the La Palisse flow: (a) from the colonnade and the entablature of  
 737 site 1, (b) from the colonnade and the layered zone of site 2 and (c) from the pseudo-colonnade of site  
 738 2. Equal area, lower hemisphere projection in the specimen coordinates system with the field

739 measured sample angles  $X$  (azimuth) and  $Z$  (dip). Contours are in Multiples of Uniform Distribution  
740 (MUD). DM is the maximum of density, (black square in pole figures); white triangle represents the  
741 "Best Axis";  $J$  is the texture index;  $N$  is the number of measurements. (d) Representative habitus of  
742 plagioclase, clinopyroxene and titanomagnetite single crystals.

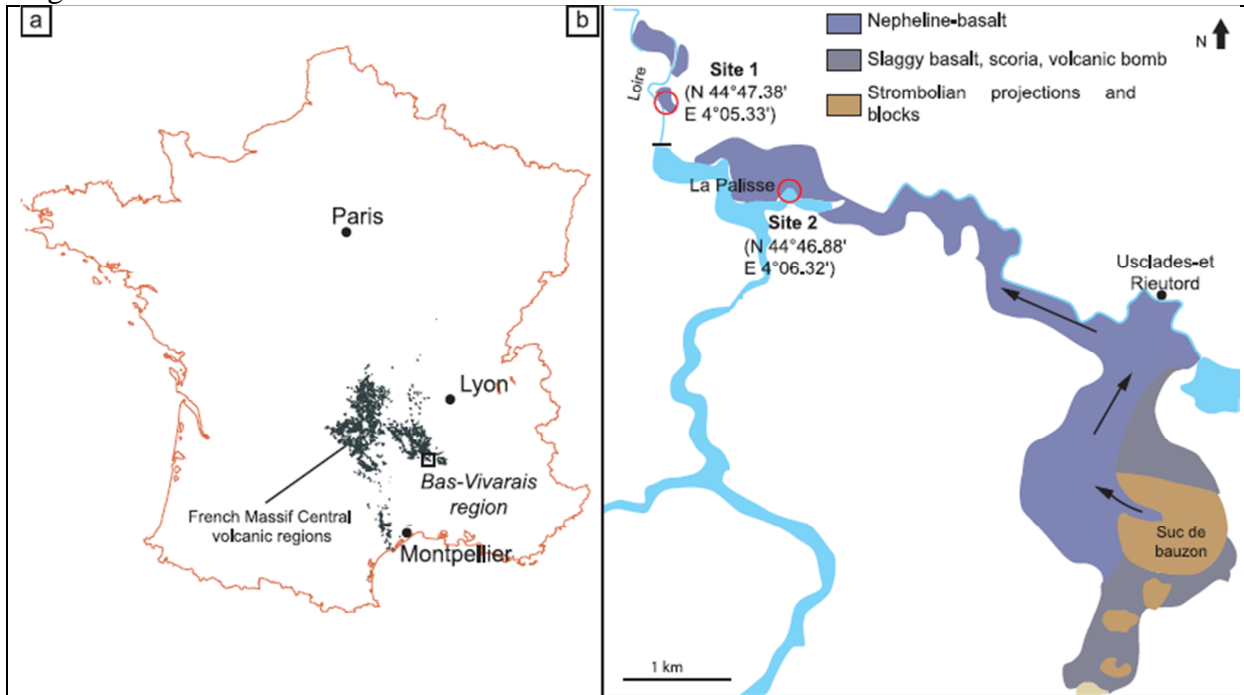
743 **Figure 10:** Projection in the specimen referential (as Fig. 9) of maximum of density (DM-Pl) and  
744 "Best Axis" (eigenvector) of plagioclase LPO for samples from the different flow levels. Maximum of  
745 density of titanomagnetite [111]-axes and mean eigenvectors  $K_1$ ,  $K_2$  and  $K_3$  are plotted.

746 **Figure 11:** (a) Projection of plagioclase LPO (maximum of density (DM-Pl) and "Best Axis") and  
747 AMS fabrics in lower hemisphere and specimen referential of 08tb14b sample from the colonnade site  
748 1, compared to the Shape Preferred Orientation (SPO) of plagioclase deduced from 2-D image  
749 analysis (rose of mean length intercepts);  $SR = 1.468$ ,  $\alpha = 76^\circ$ . (b) Projection of plagioclase LPO, AMS  
750 and 3-D plagioclase SPO of 08tb70b sample from the pseudo-colonnade site 2.

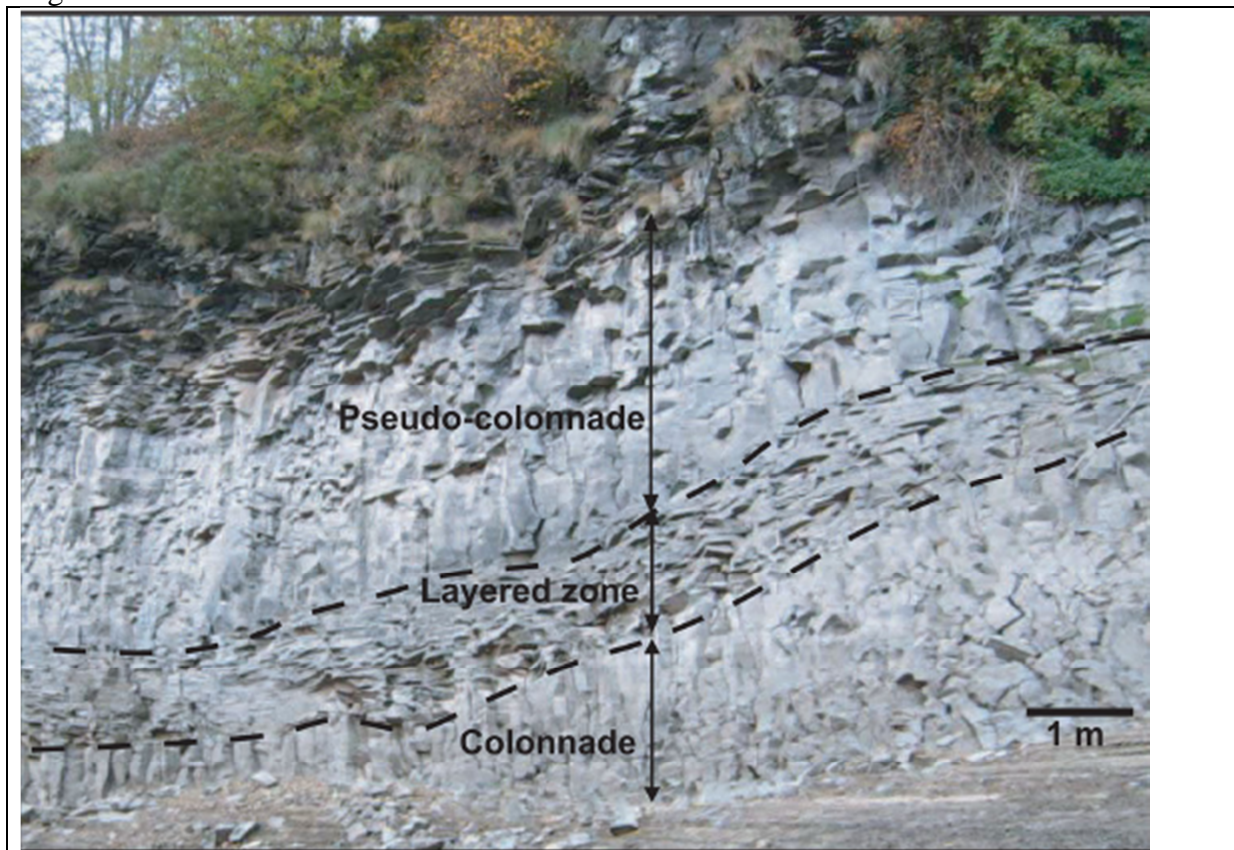
751 **Figure 12:** Principal directions of the AMS and ARM fabrics for samples from colonnade, layered  
752 zone and pseudo-colonnade, site 2 in the equal-area, lower-hemisphere projections in specimen  
753 coordinate system. The black and white symbols are AMS and ARM principal directions, respectively.

754 **Figure 13:** Summarize of site 1 and 2 characteristics (paleosurface slope, columns shape, AMS  
755 direction, magnetic properties, lattice preferred orientation of plagioclase and the relationship between  
756 magnetic and crystallographic fabric). For plagioclase SPO, S.A. indicates the Short Axis and L.A. is  
757 the Long Axis.  
758

759 Figure 1

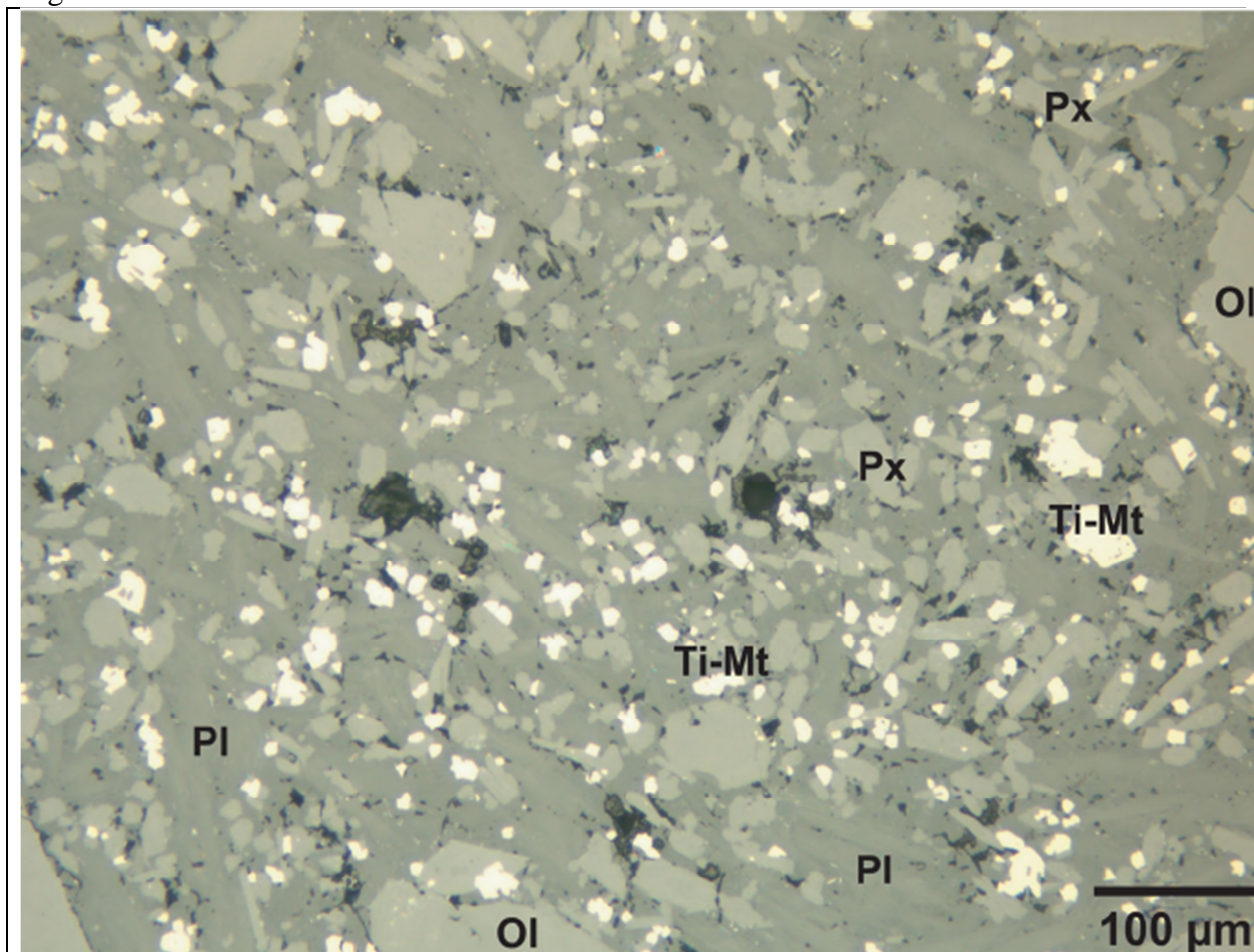


760 Figure 2



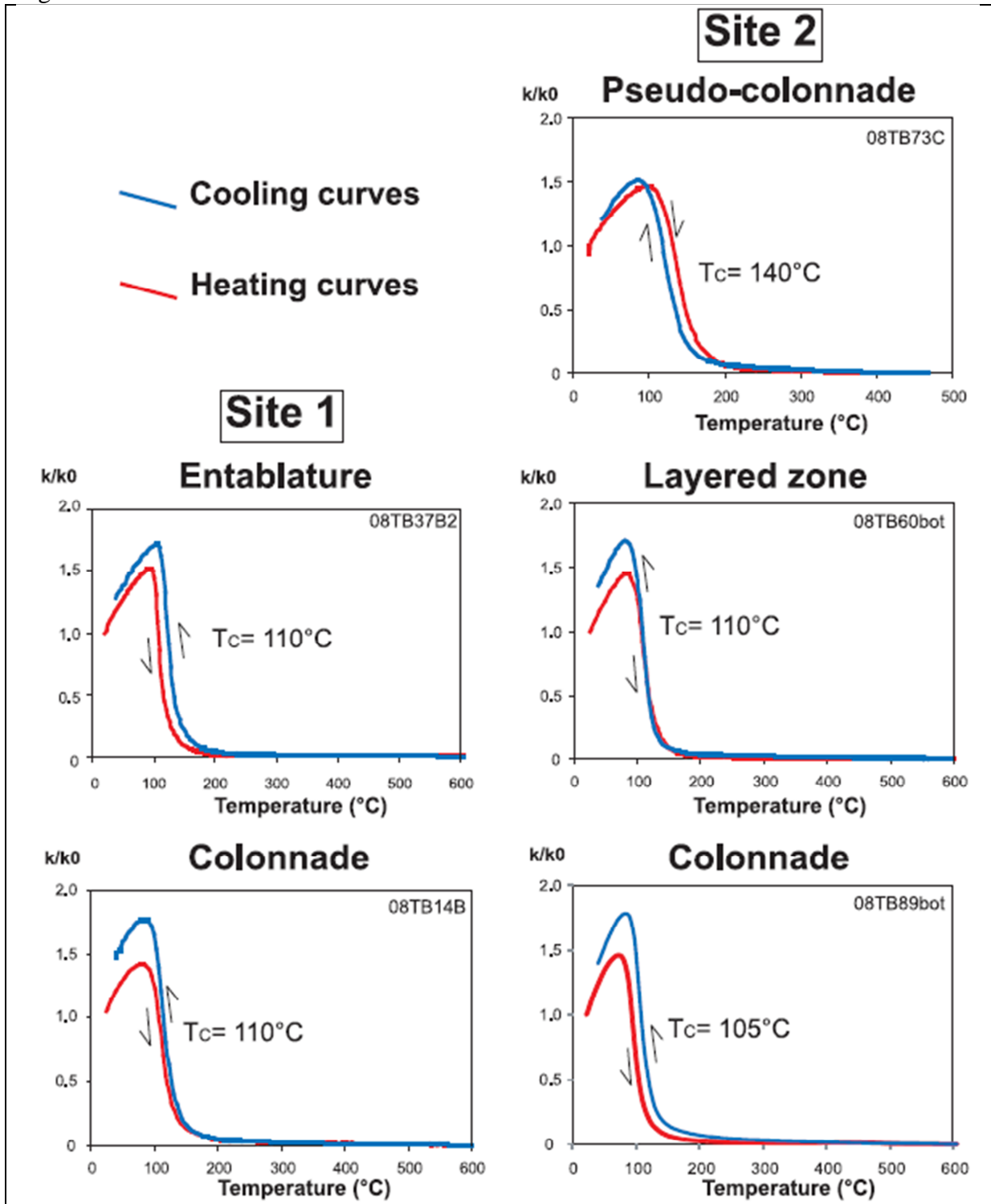
761

762 Figure 3



763  
764

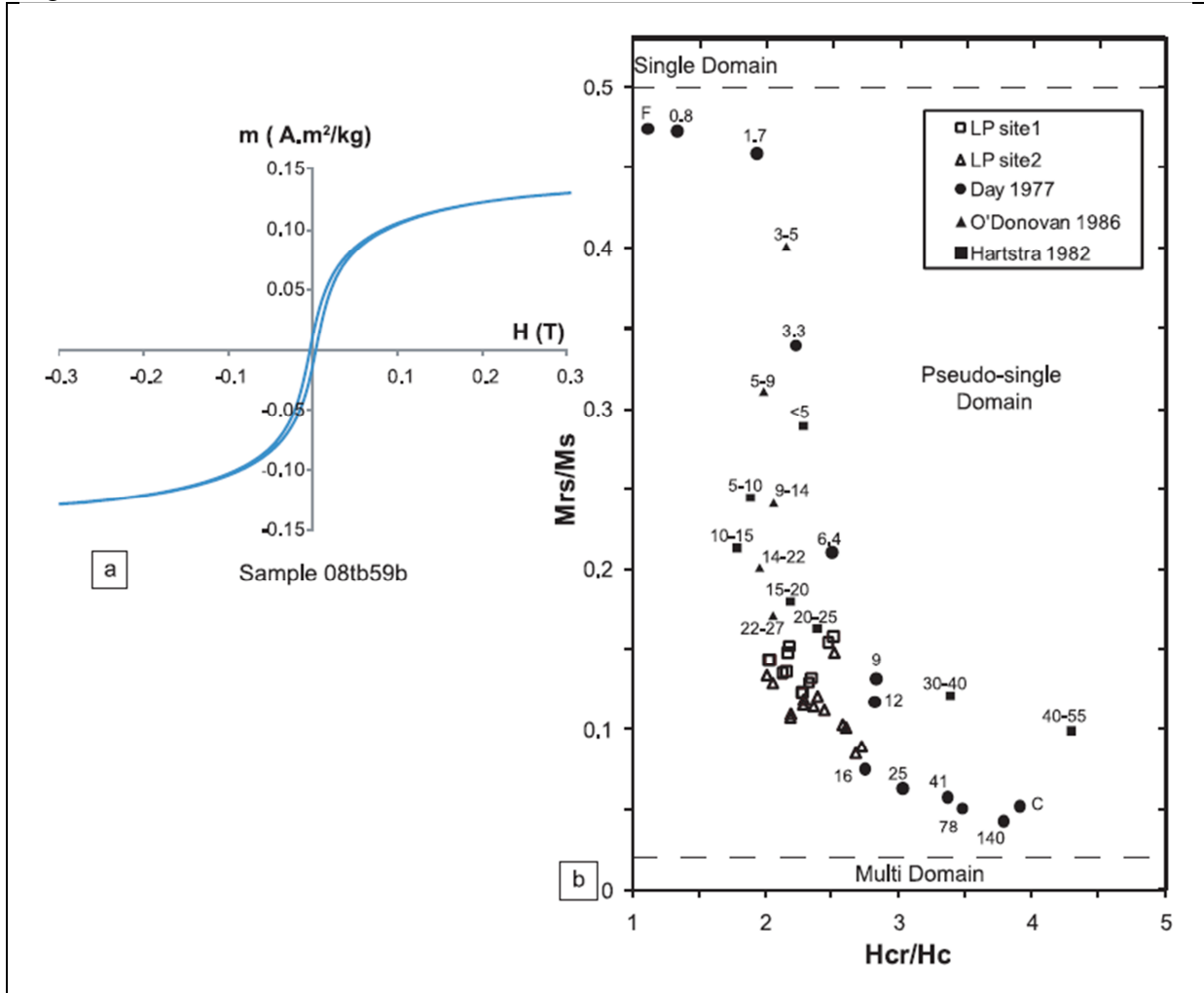
765 Figure 4



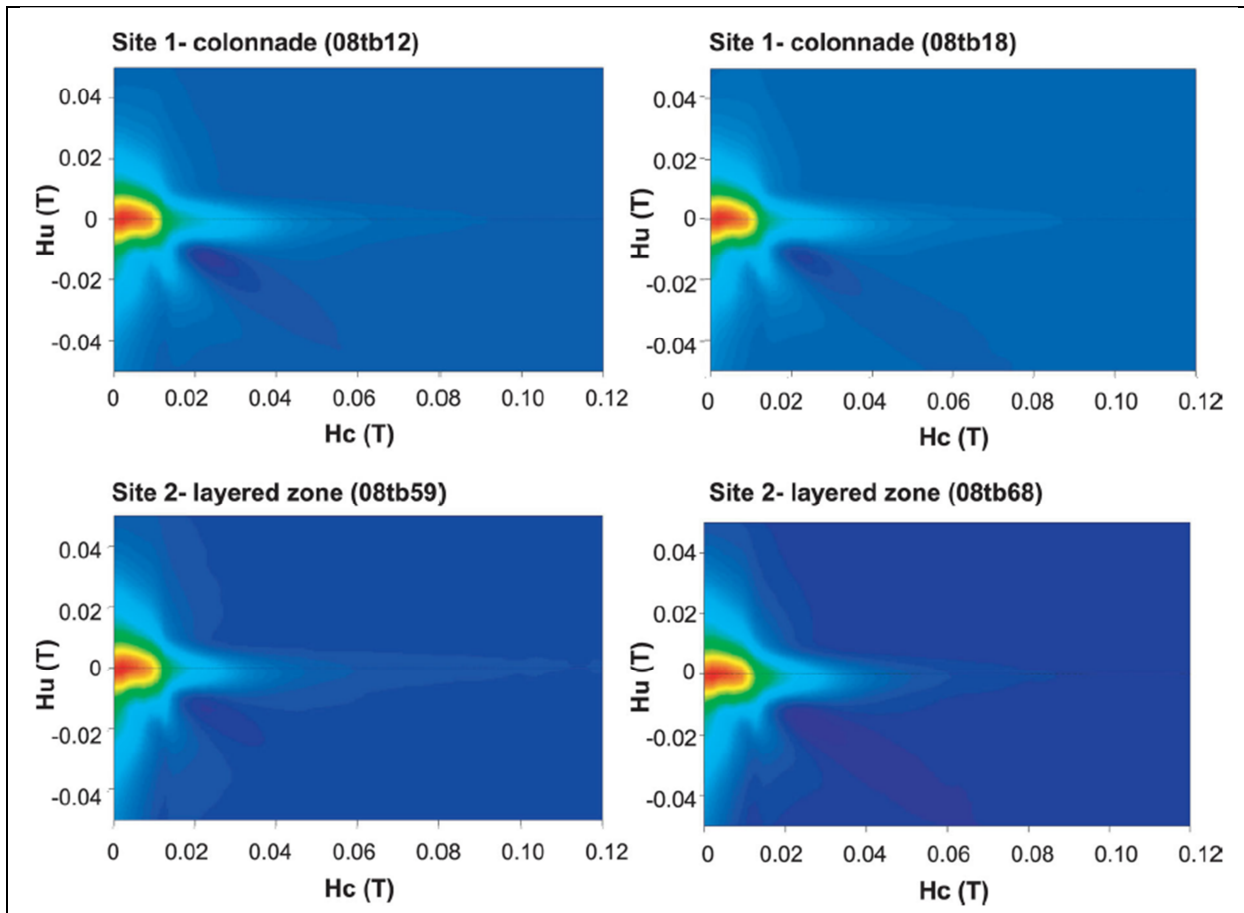
766

767

768 Figure 5



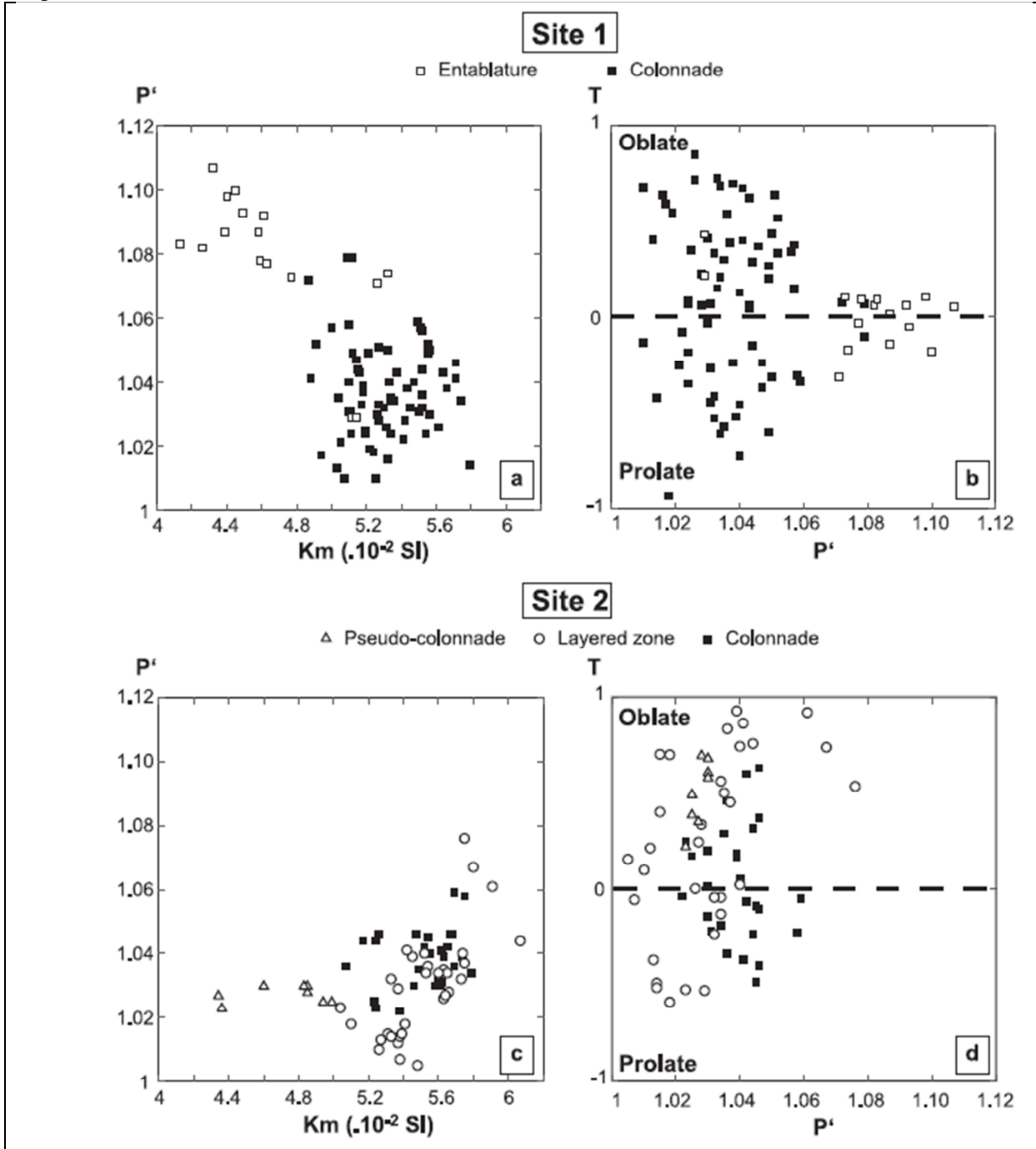
769 Figure 6



770

771

772 Figure 7

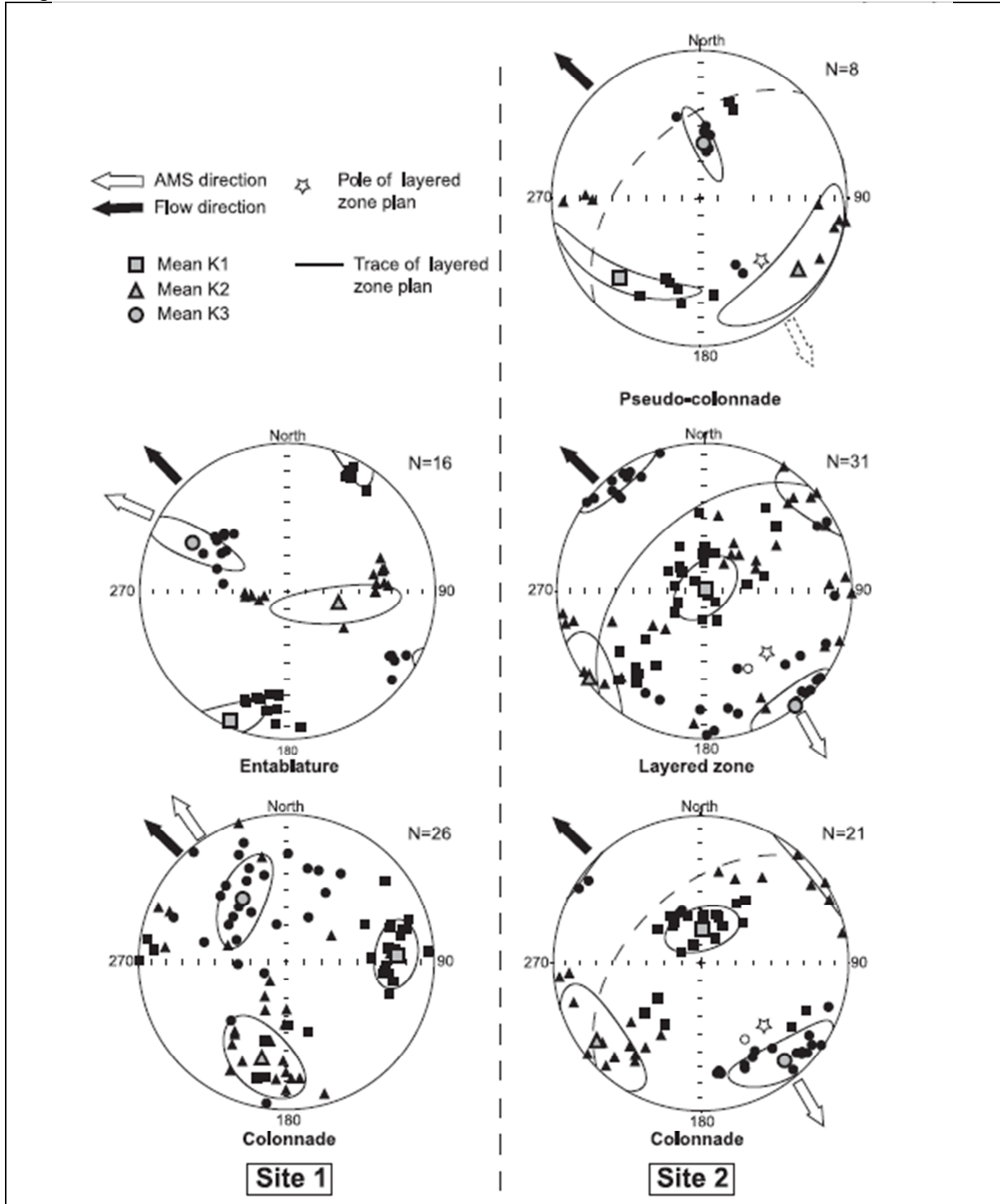


773

774



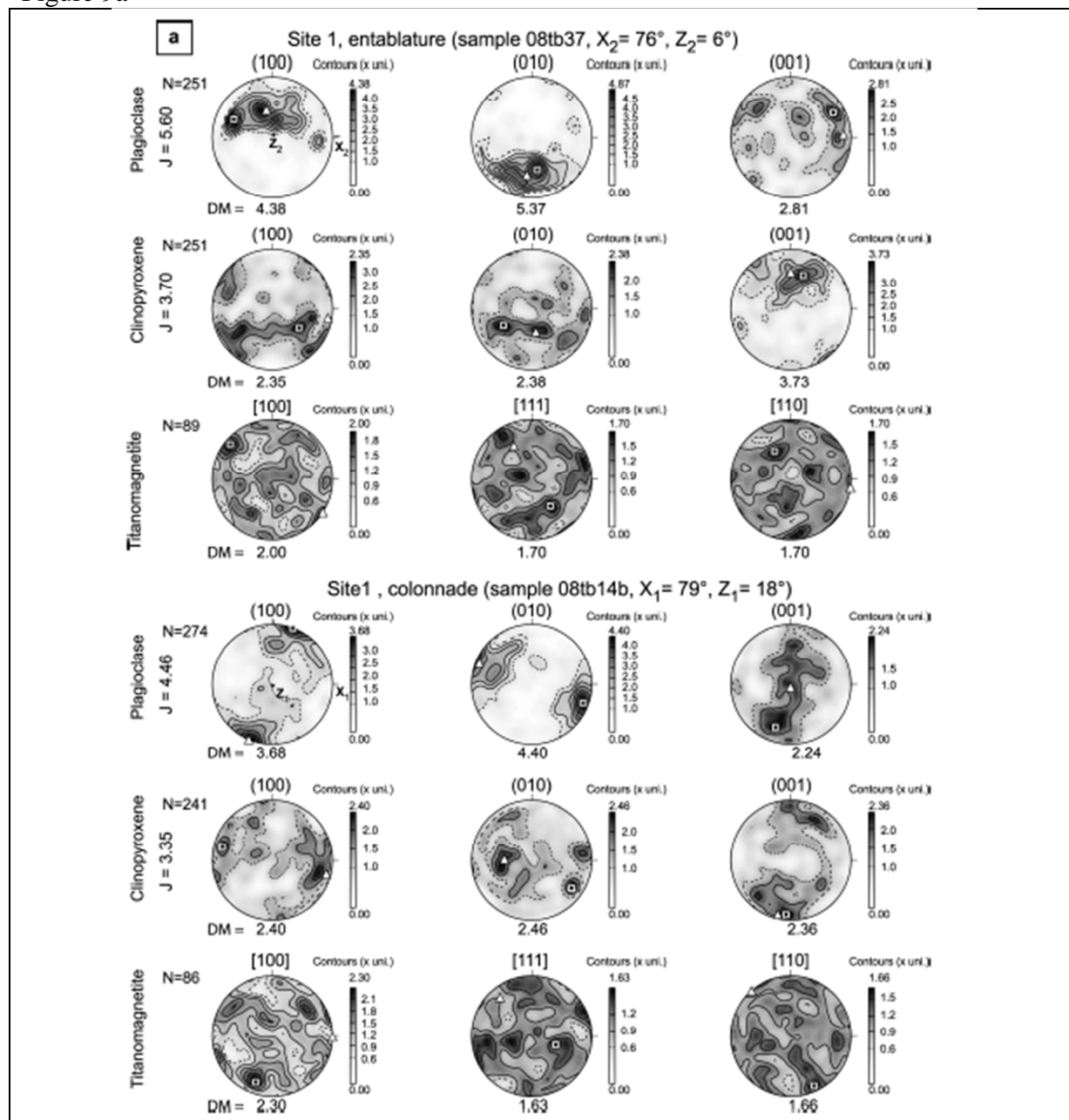
775 Figure 8



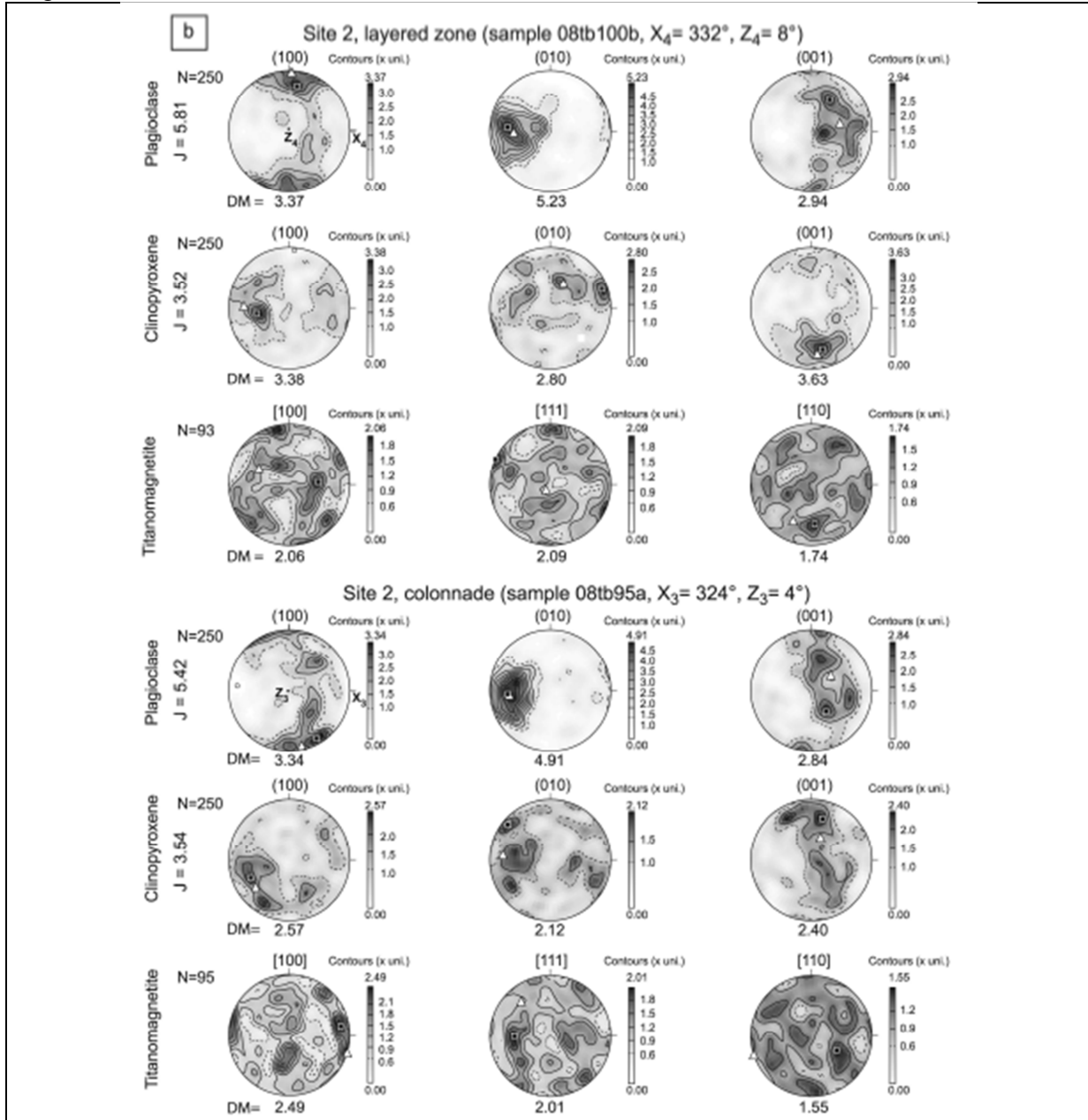
776

777

778 Figure 9a



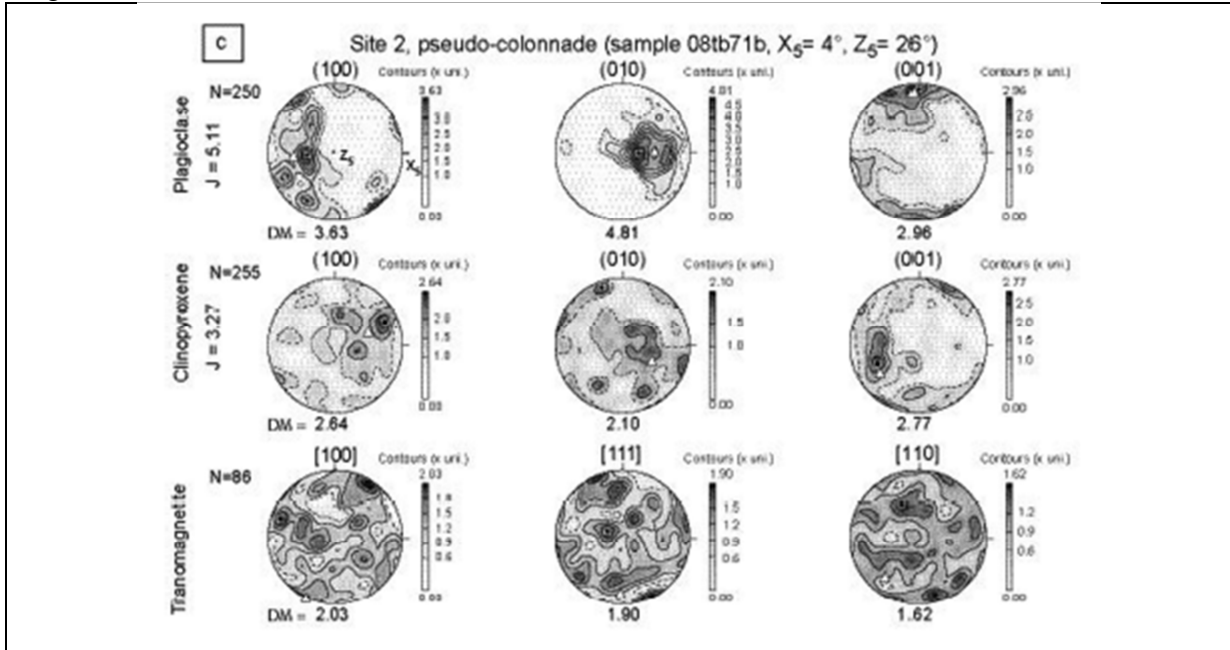
780 Figure 9b



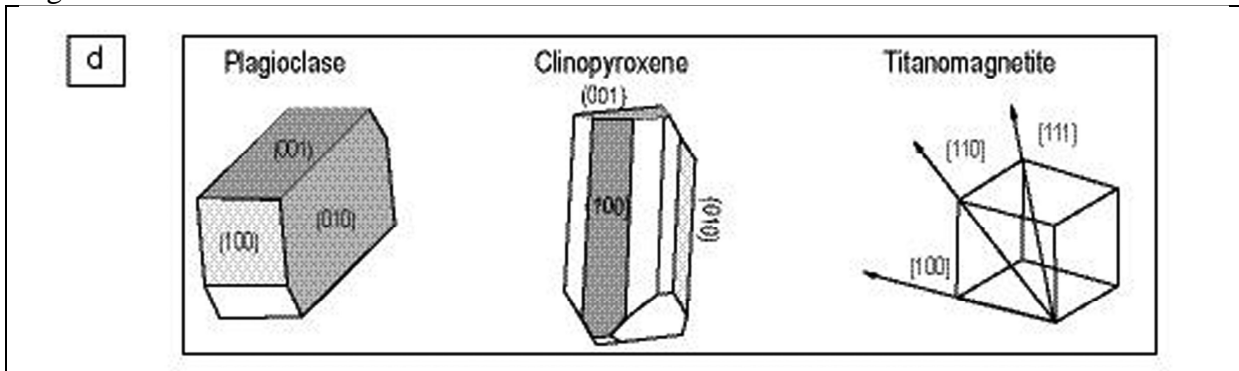
781

782

783 Figure 9c



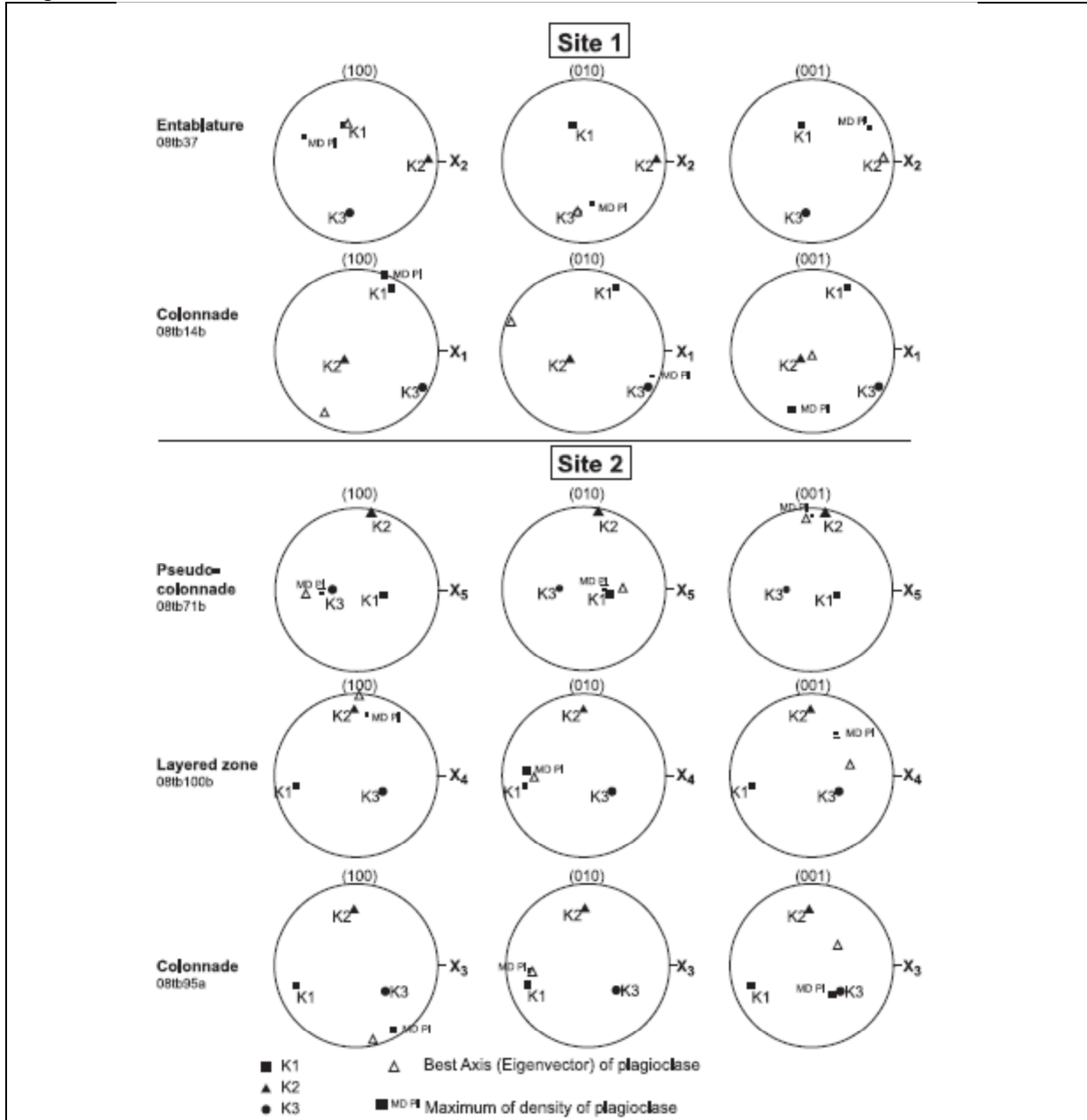
784 Figure 9d



785

786

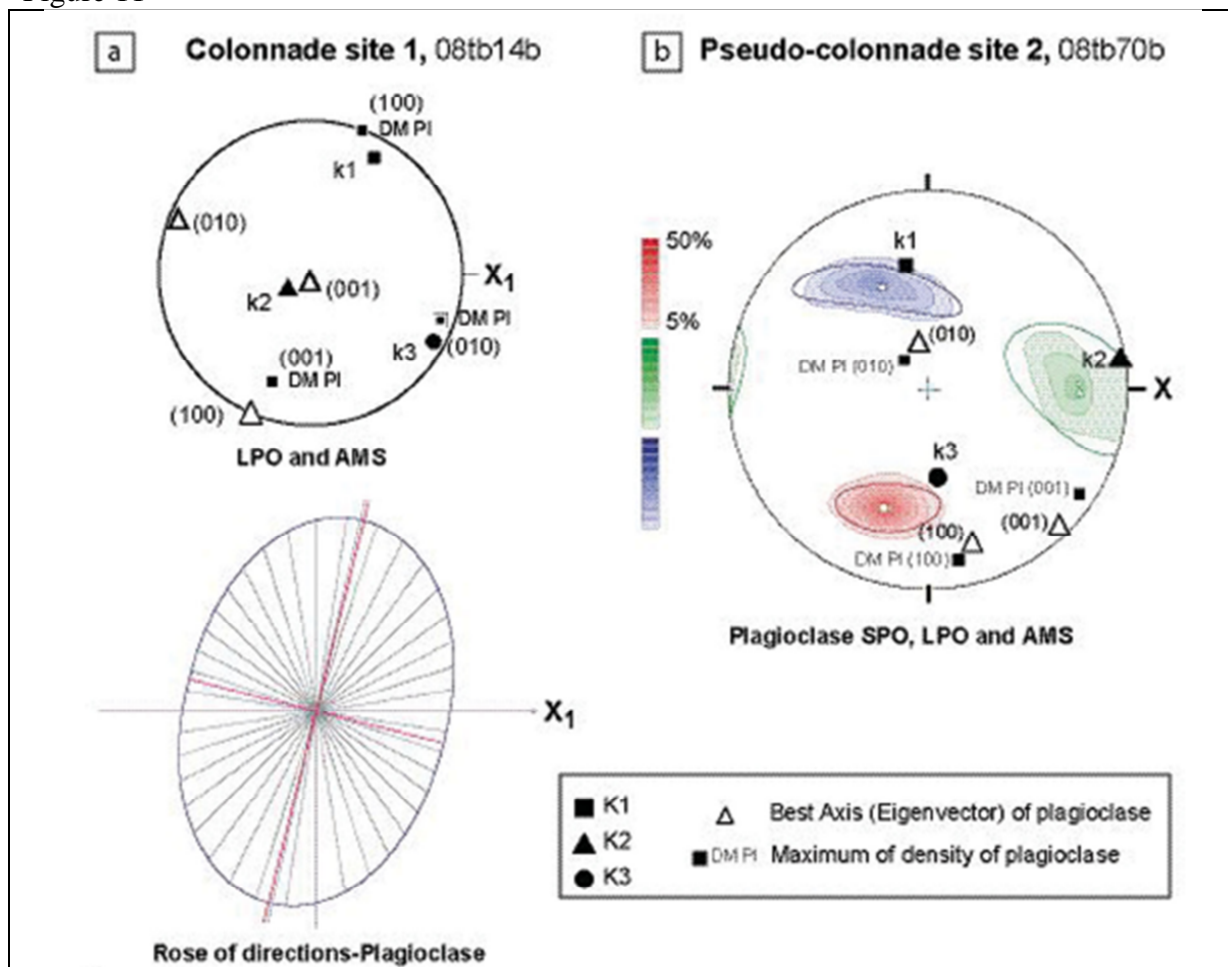
787 Figure 10



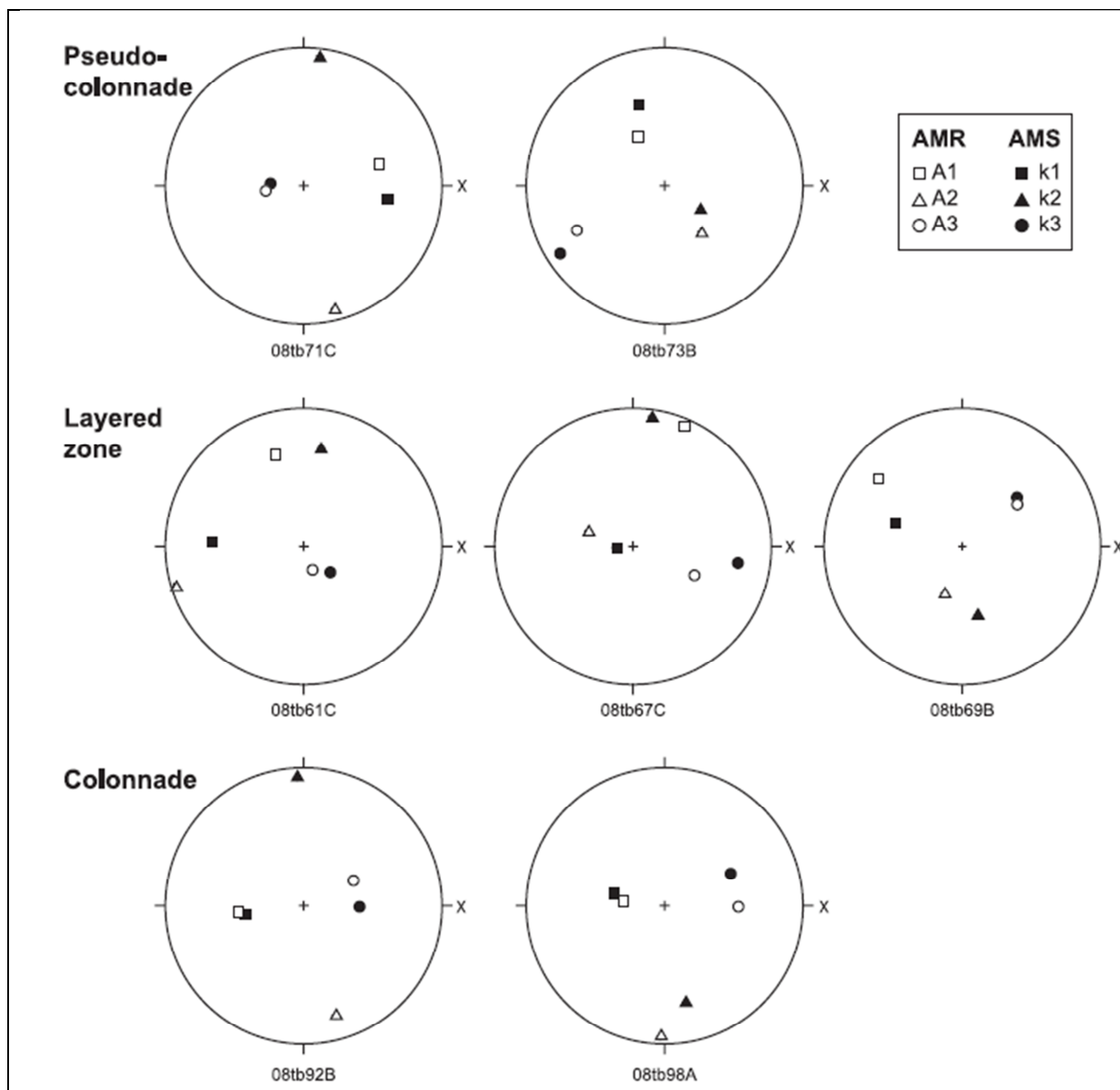
788

789

790 Figure 11



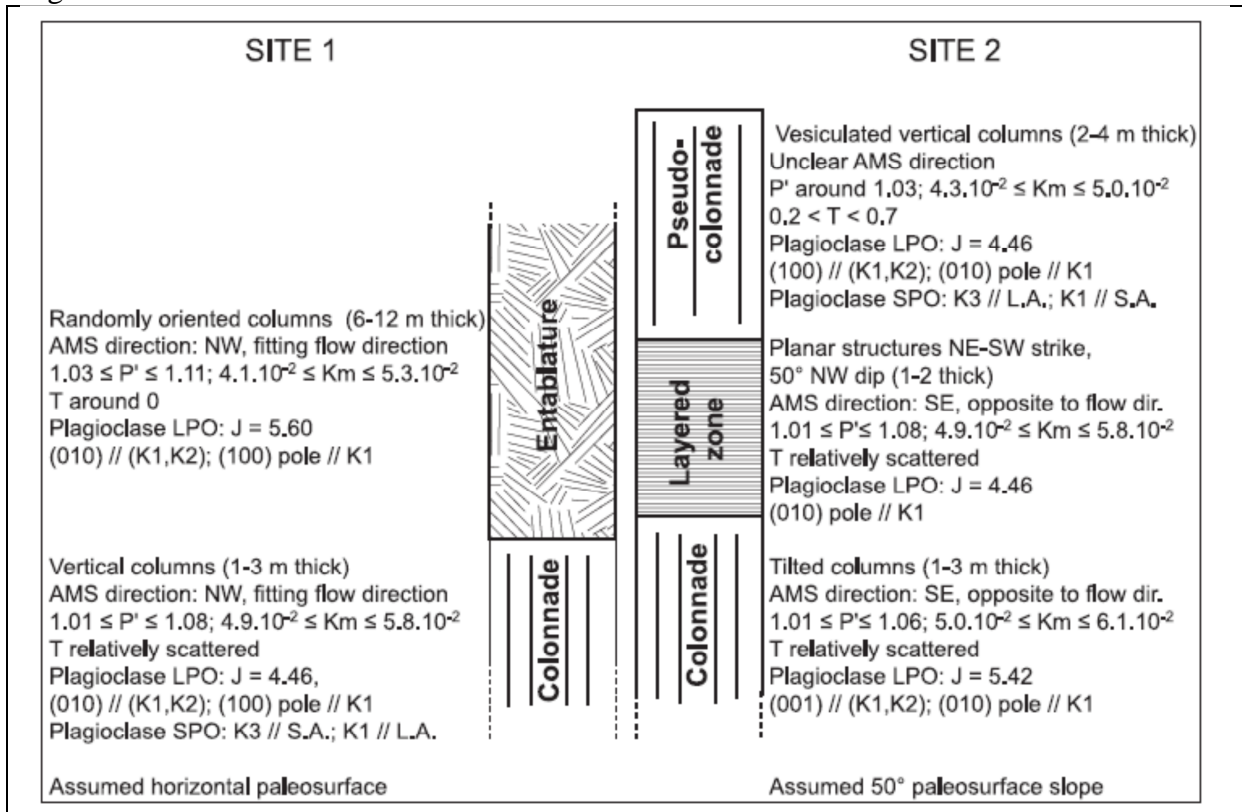
791 Figure 12



792

793

794 Figure 13



795